NIST-GCR-93-622

Transient Cooling of a Hot Surface by Droplets Evaporation

P. Tartarini
Y. Liao
M. di Marzo

Grant 70NANB8H0840

NIST

NIST-GCR-93-622

Transient Cooling of a Hot Surface by Droplets Evaporation

P. Tartarini
Y. Liao
M. di Marzo

University of Maryland
Mechanical Engineering Department
College Park, MD 20742

November 1990

Issued April 1993

Sponsored by:
U.S. DEPARTMENT OF COMMERCE
Technology Administration
National Institute of Standards
and Technology
Building and Fire Research Laboratory
Gaithersburg, MD 20899

U.S. DEPARTMENT OF COMMERCE
Ronald H. Brown, Secretary

NATIONAL INSTITUTE OF STANDARDS AND TECHNOLOGY
Raymond G. Kammer, Acting Director

Notice

This report was prepared for the Building and Fire Research Laboratory of the National Institute of Standards and Technology under grant number 70NANB8H0840. The statements and conclusions contained in this report are those of the authors and do not necessarily reflect the views of the National Institute of Standards and Technology or the Building and Fire Research Laboratory.

TRANSIENT COOLING OF A HOT SURFACE BY DROPLETS EVAPORATION

Final Report

P. Tartarini, Y. Liao, M. di Marzo

Prepared for the

Center for Fire Research

National Institute of Standards and Technology

Gaithersburg, MD 20899

Mechanical Engineering Department

Report No. 90-6

University of Maryland

College Park, Md 20742

November 1990

ABSTRACT

This report describes the research performed during the period July 1989 - July 1990 under a joint research program between the Mechanical Engineering Department of the University of Maryland and the Center for Fire Research of the National Institute of Standards and Technology. The research is conducted by Graduate Research Assistants of the ME Department under the joint supervision of Dr. di Marzo (UMCP) and of Dr. Evans (CFR - NIST).

A new experimental set-up for the study of dropwise evaporation in a radiant heat transfer field has been designed, constructed and tested. The various issues of concern such as: steady state solid temperature distribution, radiant heater design and configuration, infrared background noise and post test data manipulation are outlined.

The formulation of a model for the prediction of the cooling induced by an evaporating droplet impinging a semi-infinite solid is the subject of this report. The thermal interactions during the evaporation of a liquid droplet deposited on a low conductivity semi-infinite solid are complex because the evaporative process is coupled to the solid intense local cooling. A combined Boundary Element Method (BEM) and Control Volume Method (CVM) has been used to solve this complex numerical problem. The results for both high and low thermal conductivity materials are in excellent agreement

with the experimental findings. Detailed comparison of the surface temperature distributions on solid Macor detected with infrared thermography are also performed to demonstrate the accuracy of the computational method.

page

List of Figures

List of Tables

NOMENCLATURE

a	thickness of the droplet
c_p	specific heat
D	steam water mass diffusivity - diameter
$\mathcal{f}$	forcing and unknown vector
G	Green's function
h_a	convective heat transfer coefficient
h_{fg}	latent heat of vaporization
k	thermal conductivity
$L_o(z)$	Bessel function: $e^{-z} I_o(z)$
Le	Lewis number: $(D/\alpha)^{2/3}$
$\hat{n}$	unit vector normal to the surface
q	heat flux
r	radial coordinate
r_i	radius of influence
R	radius of the solid wetted region
s	surface
t	time
t_o	recollection time
T	temperature
T_a	far field air temperature
T_c	contact temperature defined by Seki
T_i	initial solid surface temperature
u	transformed temperature
v	volume

$\vec{v}$	position vector
V_i	initial droplet volume
W	weight matrix
x_a	far field steam in air mass fraction
x_i	interfacial steam in air mass fraction
z	axial coordinate
α	thermal diffusivity
β	ratio between the diameter of the droplet and the diameter of the corresponding spherical volume
Δr_o	spatial step
Δt_o	time step
ϵ	solid surface emissivity
Λ	latent heat of evaporation
σ	Stefan-Boltzmann constant
τ	total evaporation time

Subscripts

a	ambient, air
l	liquid
o	generic point index
r	in the radial direction
s	solid
z	in the axial direction

1. INTRODUCTION

1.1 Background

The long term objective of the study of droplet-solid interaction is to obtain information applicable to the extinguishment of fire through a droplet array (e.g. spray). The solids of concern include low thermal conductivity materials, typical of fire applications.

This report describes the research performed during the period July 1989 - July 1990 under the joint research program conducted by the Center for Fire Research (NIST) and the Mechanical Engineering Department (University of Maryland) addressing the Transient Cooling of a Hot Surface by Droplet Evaporation. This joint research program was initiated in January 1985.

The research described hereafter constitutes portion of an extensive research program aimed at developing accurate droplet cooling models of burning solid fuel surfaces. Many studies have been performed to quantify the vaporization process of both single and multi droplet arrays impacting on hot surfaces. For the studies found in the published literature, the full span of the droplet vaporization processes are usually reported. These would include evaporation, nucleate boiling, film boiling and Leidenfrost transition. This present research is more limited in the span of

vaporization process studied, being only concerned with the evaporation of single droplets on a hot surface. Limited experiments are also performed in the nucleate boiling range.

Several important results were obtained in the first years of research. In particular, the modelling of the boundary condition at the liquid-vapor interface (at the droplet exposed surface) was validated with the data collected for water droplets evaporating on an aluminum block (diMarzo 1986a, 1986b, 1988). The simple model that describes the cooling effect induced in the aluminum by the evaporating droplet (diMarzo 1986a, 1987b, 1987c) provided the input for the formulation of a preliminary multi-droplet model (diMarzo 1987a).

An extensive experimental data base was also collected for water droplet evaporating on Macor (a glass like material able to withstand strong thermal stresses). An infrared thermographic technique has been developed to monitor the temperature distribution on the surface of Macor during the evaporative process. These data are used to validate the more complex model required to describe the coupled liquid-solid interaction for the Macor case.

1.2 Overview

The rationale for the more complex coupled model has been described

at length in the previous reports. The low thermal conductivity of Macor invalidates the assumption of constant uniform temperature under the liquid droplet which was crucial in developing the simple model for the case of aluminum. This fact requires that the droplet evaporative process be solved jointly with the cooling transient in the solid.

A combined Boundary Element Method (BEM) was proposed by Dr. Baum (CFR - NIST). This method is used to integrate the solid governing equation while the liquid governing equation is solved using a Control Volume Method (CVM). The liquid-solid behavior is coupled and the solution is obtained in matrix form for the whole thermal field (solid and liquid) at once.

1.3 Program Development

In this section a brief synopsis of the various research activities is given in the time frame of the reporting period.

Period July 1989 - December 1990 Design of the new experimental set-up and requisitioning of its major components. Completion of the Macor data acquisition with the infrared thermography and preparation of the 188-89 final report.

Period January 1990 - July 1990 Derivation and implementation of the CVM method and coupling with the existing BEM for the solid in

matricial form. Code development and validation with the Macor and Aluminum experimental data. Completion of the construction and testing of the experimental set-up for the study of dropwise evaporation on Macor induced by radiant heat fluxes above the solid surface.

2. EXPERIMENTS WITH RADIANT HEAT FIELD

2.1 Radiant Set-Up Design Requirements

The initial portion of the experimental program was developed using solid materials heated by conduction from below. The heat source was an electric heater placed under the solid block which was simulating a semi-infinite solid with respect to the droplets deposited on its upper surface. A more realistic representation of a fire environment requires the semi-infinite solid to be heated from above by radiant heaters simulating flames generated by the combustion of the pyrolysis products released by the solid material.

The design requirements for the experimental set-up are:

a) uniform radiant heat input from above the solid surface capable of maintaining an initial solid surface temperature of about 200 °C

b) infrared camera unobstructed view of the droplet and of the area of surface influenced by the evaporative cooling process (up to 5 droplet diameters)

c) unobstructed access for the droplet depositor used in the previous Macor experiments for the

time required to deposit a single droplet (to limit thermal radiation damages to the dispenser)

d) uniform or linear temperature distributions in the solid at the initial steady state to satisfy the initial condition required by the BEM

e) radiant heater output control to maintain uniform conditions during the test

These design requirements were carefully considered and a balanced compromise has been achieved among the various items. In the following these various elements will be discussed and the final set-up configuration will be described in detail.

2.2 Solid Thermal Distribution Code

The first issue to be considered is the thermal configuration of the solid in its initial steady state. A simple computer code is developed to predict the temperature distribution in a block of Macor subjected to the following boundary conditions: a) radiant heat input, convection and re-radiation at the upper surface, b) convective losses at the block exposed sides, c)conduction heat losses at the bottom surface.

Note that Macor exhibits a thermal conductivity of 1.3 W/m·K which

is lower than most insulating materials. Therefore, the idea of obtaining an adiabatic boundary at the sides of the block is unpractical since one would obtain an extended surface configuration instead of an insulating barrier. To limit the losses by radiation from the solid sides, a gold paint is applied which drastically lowers the Macor emissivity.

The computations performed for a thick Macor slab show that the initial temperature profiles in the solid are not linear nor uniform. The solution to this problem is achieved by reducing the thickness of the Macor and by adding a chill plate at the bottom surface to induce a large heat transfer in the vertical direction. The radial heat flux distribution is overshadowed by the vertical component of the flux and a linear temperature profile is obtained in the central portion of the Macor solid.

2.3 Solid Geometry and Boundary Conditions

The results illustrated in the previous section dictate that a Macor slab should be used. The optimal thickness of the slab has been evaluated in the order of one inch. This thickness is large enough to retain the semi-infinite solid configuration with respect to the droplet and it provides at the same time the maximum area of linear initial temperatures required by the BEM.

The shape of the Macor block is selected as a 6 inches square tile

(one inch thick) since this configuration is readily available. The area influenced by the evaporative cooling process for a single droplet is of the order of a circle of 3 inches in radius. Therefore, the 6x6 size of the tile provides sufficient surface for the experiments. Note that the tile size is limited by the heater size and output since a uniform radiant heat condition is postulated over the whole tile surface. A reduction in radiant heat flux at the edges of the tiles will increase the steady state temperature distribution non-linearity. The convective boundary condition at the tile edge is the minimum possible heat transfer conditions that could be easily implemented. The possibility of evacuated spaces at the tile periphery has also been considered but is discarded.

The chill plate configuration does not require addition comments. The Macor tile is mounted on the chilled plate with a conductive paste to neutralize the contact resistance. The chill plate is cooled with tap water which is delivered at a constant temperature of 15 °C. The cooling water temperature rise in the chill plate is less than one °C. Therefore, the assumption of constant temperature at the Macor tile lower surface is reasonable.

2.4 Heater Design, Control and Configuration

Three conical heaters are used to provide the radiant heat input to the Macor tile. The heaters are the cone calorimeter developed at

CFR. One cone calorimeter heater was available and the other two heaters are similar in dimension and power output but much simpler in construction.

This three heaters system is connected to a three phase 220 volts power supply in a delta configuration. Two heater elements are identical and the third is very close to the other two. This provides a balanced electrical load.

The power supply is driven by an automatic controller which senses the heaters average temperature through three thermocouples and reference it to the set-point. This system is able to maintain constant heater temperature which results in a stable steady state Macor surface temperature. The Macor surface temperature that can be achieved with chilled plate cooling water at about 10 °C is in the order of 170 °C which is satisfactory for the evaporative cooling experiments. The heater temperature required for this Macor surface temperature is in the order of 750 °C.

Higher surface temperatures are achievable if the chilled plate under the Macor tile is not in operation. This is at the expenses of the uniformity of the initial surface temperature which is a condition that must be met for the exact evaluation of the evaporative cooling when the experimental data is compared with the prediction of the coupled solid-liquid model. This model is not used for the nucleate boiling regime of vaporization which occurs

at temperatures in excess of 160-170 °C.

2.5 Infrared Image Shielding From Background

Information on the transient thermal behavior of the Macor tile, of the droplet vaporization and on its size are gathered via an infrared camera which sends the information to a tape recorder.

The infrared thermography of the irradiated surface is complex since reflection is also present (the Macor emissivity was found to be equal to 0.94). To shield the camera input from most of the reflective input the portion of the surface of concern is seen through a chilled pipe.

The chilled pipe is constituted of a coiled copper tubing painted with a high emissivity paint (approximating a black body) and insulated on the outside. This pipe effectively absorbs all the stray and diffused radiation thus sending to the camera only the direct radiation incoming from the portion of the Macor surface in sight.

With this set-up a steady state uniform temperature profile is observed in all the field of view. By repositioning the three heaters carefully most of the reflection is kept out of the camera yielding meaningful information.

The transient thermography of the surface Macor surface is recorded. At selected time during the droplet evaporation one recorded frame is isolated and digitized. This digitized information is then used as input to the post-test code.

2.6 Post Test Code Modifications

The code previously developed was able to differentiate between meaningful information and noise and could provide some curve data fitting correlations.

A new code is available which doubles the data used in the surface temperature curve fitting routine and provides a better resolution for the measurement of the droplet size. This code will be used for the data reduction.

2.7 Notes and Procedures

We are currently studying the effect of placing a water droplet on a surface which is heated from three heaters. The radius of influence, time of evaporation, and the temperature profile induced by the water droplet on the heated surface at various times into the evaporation process are all important parameters which will be addressed. The setup and the experimental process will be discussed.

2.7.1 Setup

The first step in setting up the experiment is to determine a proper heater setup. The heaters should produce as uniform as possible radiant heat flux on the macor surface. It has been discovered that, although the macor has a very high emissivity (0.94), there is a non-negligible reflection off of the surface due to a very high incident heat flux. When a heater is placed facing the infra-red camera, the reflection is increased. Although the amount of reflection can be measured to a fair degree of accuracy, it is better to minimize the amount of reflection into the camera lens. After all the purpose of the camera is to see the emitted heat flux, not the reflected heat flux. For this reason, it is advisable not to place a heater opposite of the camera. The heaters cannot interfere with the placing of the water droplets. The water droplets are placed by a device which rolls in and out of the setup via two aluminum tracks. The camera is placed across from where the droplet dispenser rolls towards the setup. This way, the heaters are free to be placed anywhere except across from the camera. Two of the heaters are placed facing perpendicular to the camera's line of sight. This way reflection is minimized and since they are directly opposite of each other, they produce a uniform heat flux on the surface. The third heater is placed on the same side of the macor block as the camera. It is placed further away then the other two heaters. The camera looks through a hollow tube made up of a refrigeration coil. The tube is used to allow the camera to look directly onto the macor surface while preventing the camera from

viewing extraneous radiation from the surroundings. The tube has its inside painted black and has cold tap water flowing through it in order to minimize the amount of infra-red emitted from its surface. The macor block is attached to a plate with cold water flowing through it with heat sink compound. This maintains a cold temperature underneath the macor block. Ideally, all heat which is absorbed by the macor block would be conducted downward into the cold plate. If no heat is being conducted across the surface of the plate, there is a uniform temperature across its surface. In order to aid in this, the sides of the macor block are gold plated, so that there is very little heat transferred via radiation from the sides.

2.7.2 Procedure

The first step is to de-gas the water. If gasses are present in the water, the gasses will accumulate on the heated surface and effect the heat transfer mechanisms taking place during the evaporation process. The de-gassing is done by repeatedly freezing and melting the water while the air in the water container is being vacuum pumped. This needs to be done about once a week. The heaters are turned on and their temperature is adjusted so that the surface reaches the desired steady state temperature. Obtaining the actual surface temperature is done via a procedure described in the appendix. The infra-red camera is properly adjusted via calibration from a blackbody source. The camera is recalibrated about once a week. Once the proper surface temperature is reached and the camera

is ready, droplets can be placed. Droplets at sizes of 10,30 and 50 microliters are placed at various temperatures. About 10 droplets of each size at each temperature are placed so that an average can be taken. A VCR records the temperature profile about each of the droplets as a function of time elapsed. Each of the droplets has its temperature profile captured onto a computer disk at several different times into the evaporation process. This is done using a "Computer Eyes" software package. The runs are then curve fitted using a C language program which fits an exponential curve to the temperature profile. The program first displays the temperature profile vs. location on the macor block. The user then locates the position of the droplet using a mouse. The profile then inverts one half of the image onto the other half of the image. Since the temperature profiles are symmetric about the water droplet, this produces the effect of having twice as many data points. Next, the user selects two points, between which, a curve is to be fit. The curve fitting program produces two coefficients, which are a function of screen coordinates. Another program then converts the screen coordinate coefficients into coefficients in term of inches or millimeters. The evaporation times are measured with a stop watch. The radius of influence is obtained from the curve fit to the temperature profile.

3. MODEL OF DROPLET/SOLID INTERACTIONS

3.1 Review of Boundary Element Method

The conduction equation describes the thermal transient in a solid and in a motionless liquid. The full description of the problem requires the identification of all the boundary conditions and the coupling of the liquid and solid regions at the wetted surface under the droplet (see Fig.1). The conduction equation can be written for both the liquid and the solid, keeping in mind that the thermal diffusivity should be changed accordingly, that is:

$$\frac{\partial T}{\partial t} = \alpha \nabla^2 T \qquad (3.1.1)$$

The liquid region is bounded by a liquid-vapor interface where the mass transfer is coupled with the heat transfer as extensively described in the previous reports. This boundary condition can be summarized as:

$$-k_l \nabla T + h_a (T_a - T) = 0.624\, h_a \left(\frac{D}{\alpha_a}\right)^{\frac{2}{3}} \frac{h_{fg}}{c_{pa}} \frac{x_i - x_a}{1 - x_i} \qquad (3.1.2)$$

The liquid-solid boundary conditions express the continuity of the temperature and the conservation of energy across the interface, namely:

$$k_l \nabla T_l = k_s \nabla T_s \qquad (3.1.3)$$

$$T_l = T_s \qquad (3.1.4)$$

The boundary condition at the solid-air interface accounts for the convective and radiative heat transfer contributions:

$$-k_s \nabla T = h_a (T - T_a) + \sigma \varepsilon (T^4 - T_a^4) \qquad (3.1.5)$$

The axis-symmetric nature of the problem grants that, both in spherical and cylindrical coordinates, the gradient of T is zero on the vertical axis through the origin of the coordinate system. The initial condition can be a linear one-dimensional temperature distribution in the solid and uniform temperature in the liquid or uniform temperatures in both liquid and solid.

The droplet induced cooling of a semi-infinite body has a dual time-spatial parametric description. One could select as characteristic length some length related to the droplet wetting surface or the ratio of the solid thermal conductivity to the convective heat transfer coefficient solid-to-air or even some mixed defined length, such as the so called 'penetration length' ($l = [\alpha\ t]^{0.5}$) where the time could be the droplet evaporation time and α is the solid thermal diffusivity. Similarly the time scale could be the evaporation time or a grouping of solid related properties such as $[(\rho c_p\ k)/h^2]$ or again a mixed definition such as the square of some length related to the droplet wetting surface over the solid thermal diffusivity. The point of all this discussion been that non-dimensionalization of the governing equation is not univocal and it should not be pursued at this

preliminary stage.

The difficulties encountered in the application of differential methods to the solution of the coupled solid-liquid thermal transient suggest that a different approach should be considered. Two major considerations lead to the selection of the appropriate methodology: a) the relevant event are taking place on the surface of the domain; b) the nature of the problem with its sharp localized changes in the thermal gradient requires an integral approach.

The idea of reducing the problem to a surface problem is appealing because only the points on the solid (and liquid) surface can be monitored experimentally. An infrared thermographic technique will be used to monitor the surface temperature during the droplet evaporation transient. This technique is non-intrusive and is highly suitable to this particular problem.
Therefore, the computation limited to the surface points is more efficient and allows a more precise definition of the noding in the region of concern (e.g. at the droplet outer edge).

An integral methodology is also desirable because the solution at a given point (e.g. point temperature) is obtained by superimposing a large number of contributions from the neighboring points hence the localized, drastic thermal changes of this cooling process are smoothed out. When a finite difference technique is used the sharp

gradients are locally amplified thus causing the observed instabilities in the solution.

To obtain the desired result, it is necessary to introduce an adjoint equation in terms of the Green's function 'G', that is:

$$\frac{\partial G}{\partial t} = -\alpha \nabla^2 G \qquad (3.1.6)$$

By multiplying Eq.(3.1.1) by G and Eq.(3.1.5) by T respectively and integrating over the domain making use of Gauss' theorem, one obtains:

$$\int_t \int_v \frac{\partial (TG)}{\partial t} \, dv dt = \alpha \int_t \oint_s (T \nabla G - G \nabla T) \cdot \hat{n} \, ds \, dt \qquad (3.1.7)$$

At this point the left-hand-side is expanded into two volume integrals at time t and at time zero respectively. By G at time t and on the boundary as the Dirac function, the volume integral at time t reduces to T. Further, one can introduce a new variable u in lieu of the temperature which is zero in all the volume at the initial time (t = 0). For instance one can define u as:

$$u = T - T_0 - \frac{qz}{k_1} \qquad (3.1.8)$$

With these two modifications the final result is achieved in the form:

$$u = \alpha \int_t \oint_s (G\nabla u - u\nabla G)\cdot\hat{n}\, ds\, dt \qquad (3.1.9)$$

This integral is performed over a closed surface. However, the surface bounding the solid region below the plane z=0 is far ahead of the advancing thermal wave. Therefore, the contribution of the points on the surface bounding the domain in the far field is negligible. With the implementation of the cylindrical coordinate system, the equation is further simplified since the angular integration can be expressed in terms of a Bessel function. The final forms results in a double integral in time and along the radius 'r' which can be cast as follows:

$$u(r,t) = \frac{1}{\sqrt{4\pi\alpha}} \int_0^t \int_0^\infty \nabla u(r_0, t-t_0)\, r_0\, t_0^{-\frac{3}{2}}\, L_0\left(\frac{2 r r_0}{4\alpha t_0}\right) \exp\left(-\frac{r^2 - r_0}{4\alpha t_0}\right) dr_0\, dt_0 \qquad (3.1.10)$$

In order to simplify the task of handling these complex surface integrals, a decomposition in two portions is proposed: the value of the forcing function or of the unknown function (∇u) is assumed to be constant in the small intervals dr_0 and dt_0. This introduces formal errors of the order $(dr_0/R)^2$ and $(dt_0/t)^2$ into the analysis. The various surface integrals can be recast in the following useful form:

where 'W' is a weight matrix and 'f' is the vector of the forcing and unknown functions.

$$u = \sum_{i=1}^{n} W \cdot f + W_0 \cdot f_0 \qquad (3.1.11)$$

The summation term is known since it involves previously calculated parameters. The second term on the right-hand-side of Eq.(3.1.10) contains unknown functions and the specified boundary conditions.

In general, each solution at a given point depends on the effects of all the other surface points. So far the effect of points belonging to the same surface have been considered. The inter-surface dependance will require special treatment as described later with the presentation of the final solid-liquid coupled model. More immediate consideration must be given to peculiar situations: the effect of the forcing function at the point of concern and the singular behavior of points at the origin of the spacial and temporal coordinates.

The first particular case of interest is when the point of concern coincides with the source point. This corresponds to the maximum influence of a source point because the distance is minimal.

In order to treat this singularity in detail, an analytical integration of the general expressions of 'G' and '∇G' is performed over the elementary portion of surface represented by one node (e.g., $(x - \Delta x/2) \leq x \leq (x + \Delta x/2)$). For the disk and the plane the result is:

$$w(r\equiv r_0, t_0) = r\, t_0^{-1}\, L_0\left(\frac{2r^2}{4\alpha t_0}\right) \operatorname{erf}\left(\frac{\Delta r_0}{\sqrt{16\alpha t_0}}\right) \Delta t_0 \qquad (3.1.12)$$

Note that the term Δt_0 is consistent with the formulation of Eq.(3.1.11) where the forcing function f is multiplied by the weight W. By comparing Eq.(3.1.11) with the general formulations for u, it is clear that a temporal and spacial integration must be performed on the weighing function. Such integration in this case is performed analytically in the space and numerically in time. The units of the weight W are those of length as expected.

About the points at time $t = t_0$, these singularities are addressed by staggering the discretization of the domain. The time discretization is not carried to the time origin (eg. the present time or $t_0 = 0$). Since the weight function is characterized by the presence of a high peak (similar to a Dirac Delta) near the time origin, the integration over the first time step has to be performed with the maximum possible accuracy, and this was done by using the most advanced mathematical routines by IMSL. The discretization of the integrand must have a resolution such that the peak of the function can be properly captured. Consequently, the behavior of the weight function for various governing parameters versus the recollection time becomes essential. In order to describe the weight function for combinations of the parameters (Δr_0, Δt_0, α), a non dimensional quantity is identified as $P = \Delta r_0^2/(\alpha \cdot \Delta t_0)$. The physical properties of different materials determine the value of the parameter P, and consequently the height

of the initial peak in the temporal behavior of the weight function. This information can be used to set properly the duration of a single time step.

In light of the previous observations it is important at this point to gain some insight in the concept of recollection time. The real time is elapsing as the evaporative cooling process takes place. The recollection time is zero at the present time and stretches its positive axis in the past. Further, the effect of past forcing functions fades as real time goes by, hence the weights of the past forcing function keep decreasing. Depending on the type of material and on the extent of the cooling, the recollection (memory) of the system is longer or shorter but in any case limited only to a finite number of previous time steps.

By rearranging the equations for all the points, one can recast the problem in the form

$$A \cdot \vec{X} = \vec{B} \qquad (3.1.13)$$

where A is the modified weight matrix at the present time. This matrix is composed of all the weights associated with the unknown fluxes and with portion of the identity matrix associated with the unknown temperatures. The vector B is a vector that encompasses known quantities at present and past times as shown in the summation term of Eq.(3.1.11). Further, B also includes the known weight-flux products or the known temperatures at the exposed surfaces (cap and plane) which are described by the boundary

conditions.

Matrix Structure. Intuitively, the weight function must have its highest value when the source coincides with the point of concern and should decay as the source moves further away from the point. This behavior is confirmed by the numerical values of several test cases. The weights can be arranged in a matrix form where each column is composed of all the weights associated with the sources affecting one single point. Similarly a row is the collection of all the weights associated to one single source affecting the various points of the domain. This weight matrix is diagonally dominant and decays on both sides of the main diagonal as shown in Table 3. Further, it is important to note that, as time elapses the weight matrix values decay rapidly and in fact after a few time steps they become negligible. This confirms that the system recollection time extends in the past for a limited number of time steps.

After the preliminary characterization, the weight function must be tested in the full range in matrix form to establish its accuracy. Some relevant differences between the shape of the matrix in the case of aluminum and the corresponding one for the case of Macor will be outlined in the following pages.

3.2 Liquid Droplet Nodalization

As the temperature changes, the volume of the droplet decreases with time because of the evaporation. Under the assumption that the radius (R) of the wet area, which is the interface between the droplet and the solid, remains unchanged during the entire transient, the thickness (a) of the droplet must decrease until the droplet is completely evaporated. Another assumption to be made is that the droplet has a shape which is a spherical segment (see Fig.2), so that the volume of the droplet can be expressed by

$$V=\frac{\pi}{6}a(3R^2+a^2) \tag{3.2.1}$$

and, knowing V and R, a can be found as

$$a=\sqrt[3]{\frac{3V}{\pi}+\sqrt{R^6+\frac{9}{\pi^2}V^2}}-\frac{R^2}{\sqrt[3]{\frac{3V}{\pi}+\sqrt{R^6+\frac{9}{\pi^2}V^2}}} \tag{3.2.2}$$

In cylindrical coordinates - r,z - the nodal points in the droplet are determined by

$$Z^2+(r-g_jR)^2 = 2\left(\frac{1-g_j}{g_j}\right)R(r-g_jR) \tag{3.2.3}$$

$$Z = \left(\frac{\frac{1}{f_i\gamma}+f_i\gamma}{4}R^2-r^2\right)^{\frac{1}{2}} - \frac{\left(\frac{1}{f_i\gamma}-f_i\gamma\right)}{2}R \tag{3.2.4}$$

where

$$\gamma = \frac{a}{R} \tag{3.2.5}$$

$$f_i = \frac{Z}{a}\Big|_{r=0} \qquad 0 \le f_i \le 1 \tag{3.2.6}$$

$$g_j = \frac{r}{R}\Big|_{z=0} \qquad 0 \le g_j \le 1 \tag{3.2.7}$$

While f_i and g_j go through from 0 to 1 separately, eq. 3.2.3 and eq. 3.2.4 give the coordinates for all points of the droplet when i=2,IM and j=2,JM+1 (see Fig.3).

By solving for r and z from eq. 3.2.3 and eq. 3.2.4, one obtains

$$r_{ij} = \frac{-a_2 + \sqrt{a_2 - 4a_1a_2}}{2a_1} \tag{3.2.8}$$

and

$$Z_{ij} = \beta_1 + \beta_2 r_{ij} \tag{3.2.9}$$

where

$$\beta_1 = \frac{1 + g_j^2 + 2(1-g_j)}{\frac{1}{f_i\gamma} - f_i\gamma} R \tag{3.2.10}$$

and

$$\beta_2 = -\frac{2\left(g_j + \frac{1-g_j}{g_j}\right)}{\frac{1}{f_i\gamma} - f_i\gamma} \qquad (3.2.11)$$

$$a_1 = 1 + \beta_2^2 \qquad (3.2.12)$$

$$a_2 = 2\left[\beta_1\beta_2 - \left(g_j + \frac{1-g_j}{g_j}\right)R\right] \qquad (<0) \qquad (3.2.13)$$

$$a_3 = \beta_1^2 + [g_j^2 + 2(1-g_j)]R^2 \qquad (3.2.14)$$

For points of j=1, i=1,IM+1 which are symmetric to z-axis,

$$r(i,1) = -r(i,3) \qquad (3.2.15)$$

$$Z(i,1) = Z(i,3) \qquad (3.2.16)$$

For fake points underneath the interface, which is symmetric to r-axis,

$$r(IM+1,j) = r(IM-1,j) \qquad (3.2.17)$$

$$Z(IM+1,j) = -Z(IM-1,j) \qquad (3.2.18)$$

Above the droplet surface there is another layer, i=1 and j=1,JM+1. The expression of r_{ij}, Z_{ij} can be given by letting f_i=1 and substituting a_0 to a in eq.3.2.5, where

$$a_0 = a + [Z(2,2) - Z(3,2)] \qquad (3.2.19)$$

for eq. 3.2.3 and eq. 3.2.4

3.3 Control Volume Method Formulation

The conduction equation for the droplet without the consideration of radiation effects is expressed by the Fourier's law

$$\frac{\partial T}{\partial t} = \alpha \nabla^2 T \qquad (3.3.1)$$

where T is defined as the temperature difference between the droplet and air:

$$T = T_{droplet} - T_{air} \qquad (3.3.2)$$

By integrating over the volume of the droplet and applying the Gauss' theorem for the right hand side term of the eq. 3.3.1

$$\int_V \frac{\partial T}{\partial t} dV = \int_S \alpha \nabla T \cdot \vec{n}\, dS \qquad (3.3.3)$$

Noting in cylindrical coordinate,

$$dV = 2\pi r\, dA; \qquad dS = 2\pi r\, dl \qquad (3.3.4)$$

one has

$$\int_A \frac{\partial T}{\partial t} r\,dA = \int_L \alpha \nabla T \cdot \vec{n}\, r\, dl \qquad (3.3.5)$$

or

$$r_O \frac{\Delta T}{\Delta t} dA = \alpha \left[\frac{T_E - T_O}{\Delta \overline{x}_E} l_{AB} \frac{r_A + r_B}{2} + \frac{T_N - T_O}{\Delta \overline{x}_N} l_{BC} \frac{r_B + r_C}{2} + \frac{T_O - T_W}{\Delta \overline{x}_W} l_{CD} \frac{r_C + r_D}{2} + \frac{T_O - T_S}{\Delta \overline{x}_S} l_{DA} \frac{r_D + r_A}{2} \right] \qquad (3.3.6)$$

Referring to Fig.4,

$$l_{AB} = \sqrt{(r_{i+1,j+1} - r_{i,j+1})^2 + (Z_{i+1,j+1} - Z_{i,j+1})^2} \qquad (3.3.7)$$

$$l_{BC} = \sqrt{(r_{i,j+1} - r_{i,j})^2 + (Z_{i,j+1} - Z_{i,j})^2} \qquad (3.3.8)$$

$$l_{CD} = \sqrt{(r_{i,j} - r_{i+1,j})^2 + (Z_{i,j} - Z_{i+1,j})^2} \qquad (3.3.9)$$

$$l_{DA} = \sqrt{(r_{i+1,j} - r_{i+1,j+1})^2 + (Z_{i+1,j} - Z_{i+1,j+1})^2} \qquad (3.3.10)$$

$$dA = 0.25\,(l_{AB} + l_{CD})\,(l_{BC} + l_{DA}) \qquad (3.3.11)$$

$$r_O = 0.25\,(r_{i+1,j+1} + r_{i,j+1} + r_{i,j} + r_{i+1,j}) \qquad (3.3.12)$$

$$r_N = 0.25\,(r_{i,j+1} + r_{i-1,j+1} + r_{i-1,j} + r_{i,j}) \qquad (3.3.13)$$

$$r_W = 0.25\,(r_{i,j} + r_{i,j-1} + r_{i+1,j-1} + r_{i+1,j}) \qquad (3.3.14)$$

$$r_S = 0.25\,(r_{i+1,j+1} + r_{i+1,j} + r_{i+2,j} + r_{i+2,j+1}) \qquad (3.3.15)$$

$$r_E = 0.25\,(r_{i,j+2} + r_{i,j+1} + r_{i+1,j+1} + r_{i+1,j+2}) \qquad (3.3.16)$$

$$Z_O = 0.25\,(Z_{i+1,j+1} + Z_{i,j+1} + Z_{i,j} + Z_{i+1,j}) \qquad (3.3.17)$$

$$Z_N = 0.25\,(Z_{i,j+1} + Z_{i-1,j+1} + Z_{i-1,j} + Z_{i,j}) \qquad (3.3.18)$$

$$Z_W = 0.25\,(Z_{i,j} + Z_{i,j-1} + Z_{i+1,j-1} + Z_{i+1,j}) \qquad (3.3.19)$$

$$Z_S = 0.25\,(Z_{i+1,j+1} + Z_{i+1,j} + Z_{i+2,j} + Z_{i+2,j+1}) \qquad (3.3.20)$$

$$Z_E = 0.25\,(Z_{i,j+2} + Z_{i,j+1} + Z_{i+1,j+1} + Z_{i+1,j+2}) \qquad (3.3.21)$$

and

$$\Delta\overline{x_N} = \sqrt{(r_N - r_O)^2 + (Z_N - Z_O)^2} \qquad (3.3.22)$$

$$\Delta\overline{x_W} = -\sqrt{(r_O - r_W)^2 + (Z_O - Z_W)^2} \qquad (3.3.23)$$

$$\Delta\overline{x_S} = -\sqrt{(r_O - r_S)^2 + (Z_O - Z_S)^2} \qquad (3.3.24)$$

$$\Delta\overline{x_E} = \sqrt{(r_E - r_O)^2 + (Z_E - Z_O)^2} \qquad (3.3.25)$$

After simplifying, eq. 3.3.6 becomes

$$\frac{\Delta T_{ij}}{\Delta t} = a_{i,j+1}T_{i,j+1} + a_{i-1,j}T_{i-1,j} + a_{i,j-1}T_{i,j-1} + a_{i+1,j}T_{i+1,j} + a_{i,j}T_{i,j} \qquad (3.3.26)$$

where

$$a_{i,j+1} = \frac{\alpha}{r_o dA} \frac{l_{AB}(r_A+r_B)}{2\Delta\overline{x_E}} \tag{3.3.27}$$

$$a_{i-1,j} = \frac{\alpha}{r_o dA} \frac{l_{BC}(r_B+r_C)}{2\Delta\overline{x_N}} \tag{3.3.28}$$

$$a_{i,j-1} = -\frac{\alpha}{r_o dA} \frac{l_{CD}(r_C+r_D)}{2\Delta\overline{x_W}} \tag{3.3.29}$$

$$a_{i+1,j} = -\frac{\alpha}{r_o dA} \frac{l_{DA}(r_D+r_A)}{2\Delta\overline{x_S}} \tag{3.3.30}$$

$$a_{i,j} = -(a_{i,j-1}+a_{i+1,j}+a_{i,j+1}+a_{i-1,j}) \tag{3.3.31}$$

Note that all a_{ij}'s are time dependent coefficients since the geometry of the droplet, in terms of r_{ij} and Z_{ij}, vary with time.

Applying Crank-Nicolson scheme for eq. 3.3.26, and knowing all T_{ij}'s at time step n+1 being only unknowns, one can have

$$\frac{T_{i,j}^{n+1}-T_{i,j}^{n}}{\Delta t} = 0.5(a_{i,j+1}^{n+1}T_{i,j+1}^{n+1}+a_{i+1,j}^{n+1}T_{i+1,j}^{n+1}+a_{i,j}^{n+1}T_{i,j}^{n+1}+a_{i-1,j}^{n+1}T_{i-1,j}^{n+1}+a_{i,j-1}^{n+1}T_{i,j-1}^{n+1})$$

$$+0.5(a_{i,j+1}^{n}T_{i,j+1}^{n}+a_{i+1,j}^{n}T_{i+1,j}^{n}+a_{i,j}^{n}T_{i,j}^{n}+a_{i-1,j}^{n}T_{i-1,j}^{n}+a_{i,j-1}^{n}T_{i,j-1}^{n}) \tag{3.3.32}$$

Rearranging the equation above:

$$b_{i,j+1}T_{i,j+1}^{n+1} + b_{i+1,j}T_{i+1,j}^{n+1} + b_{i,j}T_{i,j}^{n+1} + b_{i-1,j}T_{i-1,j}^{n+1} + b_{i,j-1}T_{i,j-1}^{n+1} = R_{i,j} \tag{3.3.33}$$

where

$$b_{i,j+1} = -0.5\,\Delta t\, a^{n+1}_{i,j+1} \tag{3.3.34}$$

$$b_{i+1,j} = -0.5\,\Delta t\, a^{n+1}_{i+1,j} \tag{3.3.35}$$

$$b_{i-1,j} = -0.5\,\Delta t\, a^{n+1}_{i-1,j} \tag{3.3.36}$$

$$b_{i,j-1} = -0.5\,\Delta t\, a^{n+1}_{i,j-1} \tag{3.3.37}$$

$$b_{i,j} = 1-(b_{i-1,j}+b_{i,j-1}+b_{i,j+1}+b_{i+1,j}) \tag{3.3.38}$$

$$R_{i,j} = 0.5\Delta t\,(a^{n}_{i,j+1}T^{n}_{i,j+1}+a^{n}_{i+1,j}T^{n}_{i+1,j}+a^{n}_{i-1,j}T^{n}_{i-1,j}+a^{n}_{i,j-1}T^{n}_{i,j-1})$$

$$+(1+0.5\,\Delta t\cdot a^{n}_{i,j})\,T^{n}_{i,j} \tag{3.3.39}$$

For points near the edge of the droplet, all above expressions will be modified due to the shape difference of the elements (see Fig.5). The area dA of the triangle ABC is given as

$$dA = 0.25\,(l_{AB}+l_{CA})\,l_{BC} \tag{3.3.40}$$

Instead of using averaging procedures for the rectangular elements, point O, as well as point N and S, is taken as the center of gravity of triangle ABC:

$$r_O = \frac{1}{a-b}\,(Z_{i,j}-Z_{i+1,j}+ar_{i+1,j}-br_{i,j}) \tag{3.3.41}$$

$$Z_O = Z_{i,j}+b(r_O-r_{i,j}) \tag{3.3.42}$$

where

$$a = \frac{0.5\,(Z_{i,j}+Z_{i,j+1}) - Z_{i+1,j}}{0.5\,(r_{i,j}+r_{i,j+1}) - r_{i+1,j}} \qquad (3.3.43)$$

$$b = \frac{0.5\,(Z_{i+1,j}+Z_{i,j+1}) - Z_{i,j}}{0.5\,(r_{i+1,j}+r_{i,j+1}) - r_{i,j}} \qquad (3.3.44)$$

Referring to eqs. 3.3.7 - 3.3.25, l_{AB}, l_{BC}, l_{CA}, Δx_N, Δx_W and Δx_S can be found.

Again, applying the Crank-Nicolson scheme, the conduction equation for the edge points becomes:

$$b_{i,j-1}T_{i,j-1} + b_{i-1,j}T_{i-1,j} + b_{i,j}T_{i,j} + b_{i+1,j}T_{i+1,j} = R_{i,j} \qquad (3.3.45)$$

where, similarly to eqs. 3.3.34 - 3.3.39,

$$b_{i,j-1} = -0.5\,\Delta t\, a^{n+1}_{i,j-1} \qquad (3.3.46)$$

$$b_{i-1,j} = -0.5\,\Delta t\, a^{n+1}_{i-1,j} \qquad (3.3.47)$$

$$b_{i+1,j} = -0.5\,\Delta t\, a^{n+1}_{i+1,j} \qquad (3.3.48)$$

$$b_{i,j} = 1-(b_{i,j-1}+b_{i-1,j}+b_{i+1,j}) \qquad (3.3.49)$$

$$R_{i,j} = 0.5\Delta t\,(a^{n}_{i-1,j}T^{n}_{i-1,j}+a^{n}_{i,j-1}T^{n}_{i,j-1}+a^{n}_{i+1,j}T^{n}_{i+1,j}) + (1+0.5\Delta t\, a^{n}_{i,j})\,T^{n}_{i,j} \qquad (3.3.50)$$

$$a_{i-1,j} = \frac{\alpha}{r_o dA}\,\frac{l_{AB}(r_A+r_B)}{2\Delta\overline{x_N}} \qquad (3.3.51)$$

$$a_{i,j-1} = -\frac{\alpha}{r_o dA}\frac{l_{BC}(r_B+r_C)}{2\Delta\overline{x}_w} \qquad (3.3.52)$$

$$a_{i+1,j} = -\frac{\alpha}{r_o dA}\frac{l_{CA}(r_C+r_A)}{2\Delta\overline{x}_s} \qquad (3.3.53)$$

$$a_{i,j} = -(a_{i-1,j}+a_{i,j-1}+a_{i+1,j}) \qquad (3.3.54)$$

The governing equations for points on the droplet surface and points which are symmetric to Z-axis are determined by boundary conditions.

Due to phase change and convection, there are both heat flux and mass flux loss through the liquid surface; therefore, by taking energy and mass balances on the surface, one has:

$$-K_w\frac{\partial T}{\partial Z} = \left(\frac{x_i-x_a}{1-x_i}\right)\rho_a h_m \Lambda \frac{M_w}{M_a} + h(T_i-T_a) \qquad (3.3.55)$$

After simplifying and discretizing, the equation above becomes:

$$\frac{T_{2,j}-T_{1,j}}{\Delta\overline{x}} = \frac{0.624\,h}{K_w}\frac{\Lambda}{C_a}\left(\frac{D}{\alpha_a}\right)^{\frac{2}{3}}\left(\frac{x_i-x_a}{1-x_i}\right) + h\left(\frac{T_{2,j}+T_{1,j}}{2}-T_a\right) \qquad (3.3.56)$$

or in more general form

$$b_{2,j}T_{2,j}+b_{1,j}T_{1,j} = R_{1,j} \qquad (3.3.57)$$

where

$$b_{2,j} = 1-\frac{\Delta\overline{x}\,h}{2K_w}; \qquad b_{1,j} = -1-\frac{\Delta\overline{x}\,h}{2K_w} \qquad (3.3.58)$$

$$R_{1,j} = \frac{0.624\,\Delta\bar{x}\,h}{K_w}\frac{\Lambda}{C_a}\left(\frac{D}{\alpha_a}\right)^{\frac{2}{3}}\left(\frac{x_i - x_a}{1-x_i}\right) - \frac{\Delta\bar{x}\,h}{K_w}T_a \qquad (3.3.59)$$

Referring to Fig.6,

$$\Delta\bar{x} = \sqrt{(r^- - r^+)^2 + (Z^- - Z^+)^2} \qquad (3.3.60)$$

$$r^- = 0.25(r_{1,j} + r_{1,j+1} + r_{2,j} + r_{2,j+1}) \qquad (3.3.61)$$

$$r^+ = 0.25(r_{2,j} + r_{2,j+1} + r_{3,j} + r_{3.j+1}) \qquad (3.3.62)$$

$$Z^- = 0.25(Z_{1,j} + Z_{1,j+1} + Z_{2,j} + Z_{2,j+1}) \qquad (3.3.63)$$

$$Z^+ = 0.25(Z_{2,j} + Z_{2,j+1} + Z_{3,j} + Z_{3,j+1}) \qquad (3.3.64)$$

In addition, because of the symmetry of the temperature field about the center line of the droplet, the boundary condition is given by

$$\frac{\partial T}{\partial r}\Big|_{r=0} = 0 \qquad (3.3.65)$$

which can be further expressed as

$$b_{i,1}T_{i,1} + b_{i,2}T_{i,2} = R_{i,1} \qquad (3.3.66)$$

where

$$b_{i,1}=1; \qquad b_{i,2}=-1; \qquad R_{i,1}=0 \qquad (3.3.67)$$

Because of the continuity of the heat flux at Z=0, the boundary condition for liquid and solid interface is:

$$K_w\left(\frac{\partial T}{\partial Z}\right)_w = K_s\left(\frac{\partial T}{\partial Z}\right)_s \qquad (3.3.68)$$

Further discussion will be given in next section.

3.4 Coupled Model Description

In order to couple the solid and liquid parts together, the interface between solid and liquid must be focused on.

From the analysis of the boundary element method on Section 3.1, the equation for all solid surface points can be written as

$$u_k^n = \sum_j f_j^n W_{kj}^0 + r_k \tag{3.4.1}$$

where

$$r_k = \sum_{l=1}^{n-1} \left(\sum_j f_j^l W_{kj}^{n-l} \right) \tag{3.4.2}$$

By definition

$$u = T - T_s + \frac{q_0}{K_s} Z = T - T_s + \frac{h_s}{K_s} (T_s - T_a) Z \tag{3.4.3}$$

and

$$f = \frac{du}{dZ} \tag{3.4.4}$$

For exposed solid surface:

$$f = \frac{dT}{dZ} + \frac{h_s}{K_s} (T_s - T_a) = -\frac{h_s}{K_s} (T - T_s) \tag{3.4.5}$$

For interfacial points:

$$f = \left(\frac{dT}{dZ} \right)_s + \frac{h_s}{K_s} (T_s - T_a) \tag{3.4.6}$$

Applying boundary condition 3.3.68, the above equation becomes

$$f = \frac{K_w}{K_s}\left(\frac{dT}{dZ}\right)_w + \frac{h_s}{K_s}(T_s - T_a) \qquad (3.4.7)$$

where K_w/K_s is the ratio between water and solid conductivities. Again, letting T to be the temperature difference between solid surface and air, and referring to Fig.7, eq.3.4.1 can be written as

$$T_j = \sum_{k=2}^{JM} \frac{K_w}{K_s}\left(\frac{dT}{dZ}\right)_k W_{jk} - \frac{h_s}{K_s}\sum_{k=JM+1}^{JM+JE} T_k W_{jk} + r_j + (T_s - T_a)\left(1 + \frac{h_s}{K_s}\sum_{k=2}^{JM+JE} W_{jk}\right)$$

(3.4.8)

Knowing that, for interfacial points:

$$T_j = \frac{T_{IM,j} + T_{IM-1,j}}{2} \qquad (3.4.9)$$

and that, for exposed surface points:

$$T_j = T_{IM,j} \qquad (3.4.10)$$

and:

$$\left(\frac{dT}{dZ}\right)_k = \frac{T_{IM-1,k} - T_{IM,k}}{\Delta Z_k} \qquad (3.4.11)$$

one has the equation for points at the interface:

$$\left(0.5 - \frac{W_{jj}}{\Delta Z_j}\frac{K_w}{K_s}\right)T_{IM-1,j} - \sum_{k=2}^{JM/k}\frac{K_w}{K_s}\frac{W_{jk}}{\Delta Z_k}T_{IM-1,k} + \left(0.5 + \frac{W_{jj}}{\Delta Z_j}\frac{K_w}{K_s}\right)T_{IM,j}$$

$$+ \sum_{k=2}^{JM/k}\frac{K_w}{K_s}\frac{W_{jk}}{\Delta Z_k}T_{IM,k} + \frac{h_s}{K_s}\sum_{k=JM+1}^{JM+JE} W_{jk}T_{IM,k} = r_j + (T_s - T_a)\left(1 + \frac{h_s}{K_s}\sum_{k=2}^{JM+JE} W_{jk}\right)$$

(3.4.12)

and for points on the exposed surface:

$$-\sum_{k=2}^{JM}\frac{K_w}{K_s}\frac{W_{jk}}{\Delta Z_k}T_{IM-1,k}+\sum_{k=2}^{JM}\frac{K_w}{K_s}\frac{W_{jk}}{\Delta Z_k}T_{IM,k}+\left(1+\frac{h_s}{K_s}W_{jj}\right)T_{IM,j}$$

$$+\frac{h_s}{K_s}\sum_{k=JM+1}^{JM+JE/j}W_{jk}T_{IM,k}=r_j+(T_s-T_a)\left(1+\frac{h_s}{K_s}\sum_{k=2}^{JM+JE}W_{jk}\right) \qquad (3.4.13)$$

The right hand side terms of eq. 3.4.12 and eq. 3.4.13 are known values which contain the results from previous calculations. After assigning the governing equations for each point of the grid mesh, either from the conduction equation or boundary conditions, one finally has:

$$B \cdot T = R \qquad (3.4.14)$$

where T is the unknown temperature difference vector at time step n+1 which has to be found; B is a matrix containing all the assigned coefficients, while R is a right hand side vector which includes the known values (see Fig.8).

By solving the inverse of the matrix B, the solution for T at n+1 time step is given as

$$T = B^{-1} \cdot R \qquad (3.4.15)$$

Based on the newly calculated temperature field at current time, a new droplet volume can be computed from

$$V_{new} = V_{old} - \frac{dV}{dt} \qquad (3.4.16)$$

where

$$\frac{dV}{dt} = \frac{2\pi(0.624)h}{\rho_w C_a}\left(\frac{D}{\alpha_a}\right)^{\frac{2}{3}} \int_0^L \frac{x_i - x_a}{1 - x_i} r \, dl \qquad (3.4.17)$$

in which dl is an integration along the droplet surface.

A flow chart of the procedure for solving this coupled problem is given in Fig.9.

3.5 Special Issues and Remarks

3.5.1. Recollection time.

The recollection time is a parameter that has to be fixed at the beginning of each run in relation with the solid surface material. The "memory" of aluminum is totally different from that of Macor: more specifically, the sensibility of aluminum to the heat fluxes from its past history is in the order of magnitude of 1 second, while the corresponding "memory" of Macor stretches back for more than 10 seconds. Therefore, a recollection time of 10-20 seconds can be imposed to comprehend conservatively the behaviors of both aluminum and Macor.

3.5.2. Normalization of the matrix.

The matrix of the coefficients of the coupled model has to be properly normalized in order to avoid any kind of numerical problem during the inversion procedure. This is due to the composition itself of the matrix: since it is constituted by terms of very different kind and order of magnitude, its inversion without a preliminary normalization would generate an increase in the sensibility to the initial and boundary conditions and a decrease in the level of accuracy of the solution. Therefore, since the highest values are located on the main diagonal, the matrix was normalized by dividing each row by the term belonging to the main diagonal, and the same operation was performed on the vector of the

known terms.

3.5.3. Setup of initial conditions for the temperature field.

Before the beginning of the transient, the liquid temperature is imposed to be equal to the ambient temperature (20°C) everywhere, including also the fake layer underneath the liquid-solid interface. The huge heat flux corresponding to the sudden start of the transient creates a discontinuity that is strongly sensed in the numerical simulation: in the heat flux behavior, this results in an initial damping, which becomes smoother with time.

3.5.4. Edge of the droplet.

The largest variations in the temperatures and heat fluxes of the liquid occur near the edge of the droplet. In this region, some improvements in the numerical simulation could be obtained with a more refined integration path, since the nodalization chosen does not reproduce the shape of the edge as well as it reproduces the central part of the droplet. However, this kind of modification was exploratively tried and the corresponding improvements were observed to be negligible if compared with the complexity of calculations required.

3.5.5. Heat transfer coefficient.

The overall heat transfer coefficient used for the liquid surface is based on experimental measurements, from which a constant value along the whole droplet surface is given. At the same way, also the

heat transfer coefficient for the solid surface is assumed to be constant. These assumptions are perfectly reasonable for the regions where separation between only two surfaces occurs (solid-liquid, solid-air and liquid-air), but they create a mathematical discontinuity at the intersection points between all the three surfaces (at the droplet edge defined above). The sudden transition from a region of high fluxes (solid-liquid) to a region of almost negligible fluxes (solid-air) seems to behave like a step function in the numerical simulation, and this does not correspond to the physical reality of the phenomenon. Some fluctuations in the temperatures and in the heat fluxes near the edge of the droplet can be easily explained from this point of view.

3.5.6. Sensibility of the solution scheme and optimization of the matrix of coefficients.

The matrix of coefficients in the coupled model is characterized by a very particular shape, as it was previously described. This shape is univocal determined from a qualitative point of view, but a lot of input parameters, that can be chosen with a certain degree of freedom, can create some numerical discrepancies between two solutions of the same case. This was observed and analyzed in order to obtain a sort of optimization of the matrix in terms of combination between accuracy and CPU time. The results of this analysis can be summarized as follows:

1 - The meshes in the liquid grid play different roles in the solution scheme: since the heat fluxes are predominantly axial, the

vertical nodalization is more important than the horizontal one to achieve a better understanding of the temperature distribution inside the droplet.

2 - The points on the solid exposed surface are characterized by temperature gradients which decrease with the distance from the edge of the droplet; therefore, it is possible and useful to impose a discretization that starts with the same level of accuracy chosen for the region under the droplet and decreases in proportion with the distance r.

3 - The matrix lines related to the solid part of the model contain a larger number of terms than the lines related to the liquid part, and the basic characteristics of the involved equations show that, in terms of CPU time, an increase of the number of solid points is more expensive than the same increase in the liquid region.

4 - The liquid-solid interfacial points are the most delicate ones: their behavior, in terms of accuracy of prediction of temperatures and fluxes, determines the convergence of the whole solution. Their number, however, has to be the same that is chosen for the horizontal discretization of liquid and solid separately; therefore, it is important to set that number of horizontal nodes in such a way that the significant variations of the interfacial temperature are individuated without a too fine discretization.

The nodalization which was obtained as an optimized result is characterized by the following subdivisions:

- liquid height: 15 layers;

- solid-liquid interfacial segment: 6 nodes;
- exposed solid surface: 24 nodes, with the distance between them doubled every 6 nodes.

3.5.7. Numerical problems from VAX to IBM.

The code was initially implemented on the VAX3100 of the University of Maryland at College Park, and only in a second time it was implemented also on the IBM 370 at the same location. This was supposed to be a trivial transfer operation between two well known machines: in the reality, that operation turned out to be a complex procedure involving a certain number of numerical problems not always easy to be solved.

Some mathematical subroutines from the IMSL library, for instance, were found to behave differently on the two machines in relation with the number of elements of the matrix of the coefficients and of the vector of the known terms. The inversion of the matrix was the most delicate step, also because the different intrinsic level of numerical accuracy from VAX to IBM is per se a cause of little discrepancies in the corresponding truncation errors.

3.5.8. Inconsistency of the theoretical contact temperature.

The experimental and numerical results obtained for very different solid surface materials demonstrate that the theoretical contact temperature proposed by Seki et al. is a very rough approximation of the real distribution of temperature that characterizes the

interfacial behavior during the evaporative transient. The concept of contact temperature appears to be useful in terms of stability of the solution, but its numerical value is close to the real one in a very limited number of cases.

The demonstrated inadequacy of the theoretical contact temperature represents a turning point both in the calculation of the interfacial temperature distribution and in the definition of the radius of influence for the droplet. An important part of the analytical program of the next grant period will consist of substituting that contact temperature with a new reference parameter based on the interfacial heat flux.

3.6 Code Validation

The coupled model presented in 3.4 was used to reproduce numerically a large number of experimental tests provided by the infrared apparatus described in section 2. A direct comparison between numerical predictions and experimental results is possible for the evaporation time and for the distributions of temperature under the droplet and on the exposed solid surface.

The evaporation time of droplets of different size (10 ml, 30 ml and 50 ml) is the variable which gives the most consistent insight into the prediction capability of the code. Therefore, a very large number of data from tests on aluminum and Macor was collected, in a broad range of initial solid surface temperatures, and all the corresponding evaporation times were calculated by the code and eventually compared with the experimental values. The experimental values reported here are, for each case, the result of an average of the slightly different evaporation times obtained during more repetitions of the same test: this holds the margin of the experimental errors under an acceptable 5 percent.

The results of this comparison are presented in the following page (Table 1), and the remarkable agreement between experimental and numerical results is showed in Fig.10 and Fig.11, where the calculated evaporation times on aluminum and Macor are plotted versus the corresponding experimental values.

	A	L	U	M	I	N	U	M	
		50 microliters			30 microliters			10 microliters	
Initial surface		exp. evap.	calc. evap.		exp. evap.	calc. evap.		exp. evap.	calc. evap
temperature (C)		time (s)	time (s)		time (s)	time (s)		time (s)	time (s)
100		71	68		58	56		33	40
95		100	95		63	75		37	42
91		115	109		93	99		50	54
87		135	129		107	102		64	69
82		181	167		138	139		76	88
78		221	220		165	178		95	117
75		280	255		200	207		118	139
		M	A	C	O	R			
		50 microliters			30 microliters			10 microliters	
Initial surface		exp. evap.	calc. evap.		exp. evap.	calc. evap.		exp. evap.	calc. evap
temperature (C)		time (s)	time (s)		time (s)	time (s)		time (s)	time (s)
160		71	67		54	50		28	23
155		73	65		57	51		28	24
140		86	83		66	67		38	34
133		96	90		73	72		40	35
119		127	121		94	90		53	50
115		137	132		103	100		62	59
109		153	149		117	119		66	66
102		177	175		128	135		74	78
96		210	200		151	165		87	100

Table 1 - Evaporation time: comparison between experimental and numerical results for aluminum and Macor

	Aluminum	Macor
Specific Heat (J/Kg°C)	962	835
Thermal Conductivity (W/m°C)	180	1.29
Thermal diffusivity (m^2/s)	4.55×10^{-5}	6.19×10^{-7}

Table 2 - Solid Properties

The excellent agreement between experimental data and numerical predictions is evident, and a point that has to be outlined is the coherent degree of accuracy in the numerical simulation of tests performed on two materials extremely different from the point of view of their physical properties (see Table 2).
The experimental measurements via infrared camera also show that there is a sharp increase in the evaporation rate during the final part of the transient, and this is correctly reproduced by the numerical simulation.

The predictions of the distributions of temperature in the droplet and on the solid surface constitute a main test in the validation of the code, even if the experimental data are obtainable only for the solid. The calculated distributions of temperature in the liquid, however, are very useful to demonstrate that the axial heat flux constitutes more than 90 per cent of the total heat flux during the transient. In the tests on Macor, it is possible to individuate some points at the edge of the droplet where the axial heat flux drops below that 90 per cent. This is to be expected if one considers the non-uniformity of the interfacial temperature distribution (see Fig.12).

About the temperature distribution in the solid, there are two basic fields of investigation: the first one consists in the analysis of the behavior of temperature in the solid area below the droplet, the second one consists in the analysis of the cooling

effect of the droplet on the solid "far field". Both the subjects have been investigated in this research, and the main results are presented here.

Before the coupled model was obtained, the solid temperature below the droplet was a boundary condition and it was imposed to be uniformly equal to the theoretical contact temperature proposed by Seki. With the coupled model, the matricial equation that constitutes the solution procedure was set in the following form:

$$A \cdot X = B \qquad (3.6.1)$$

where A is the matrix of liquid and solid coefficients, X is the vector containing the unknown terms and B is the vector containing the known terms. The coupling of the liquid and solid models requires that the unknown terms in X are temperatures only (in lieu of fluxes under the droplet and temperatures on the exposed surface, which were the unknowns in the solid model). With this solution scheme, the calculated temperatures under the droplet were compared, case by case, with the corresponding theoretical contact temperatures: the results showed the inadequacy of the concept of contact temperature, both when the solid surface consists of a material with very low thermal conductivity like Macor (that is the lowest conductivity case considered here: k=1.29 W/m C) and when it consists of an "opposite" material like aluminum (k=180.0 W/m C). It is particularly significant to compare the temperature distributions obtained for "extreme" materials like aluminum and Macor in cases when the theoretical contact temperature is the

same. One of these comparisons is showed in Fig.13.

The temperature distribution on the exposed solid surface is the parameter that allows to estimate how far the cooling effect of the droplet is sensed by the solid. To locate the boundaries of this area of influence, it is necessary to define a reference temperature, T_{ref}, that has to be compared with the current solid temperature T during the transient: of course, it is totally arbitrary to set the limit, in the difference $(T-T_{ref})$, under which the corresponding points of the exposed surface can be considered not influenced by the cooling effect of the droplet.

At the beginning of these researches, it was decided to define a "radius of influence" by using the theoretical contact temperature as a reference temperature. More precisely, given the initial solid temperature T_i and the theoretical contact temperature T_c, it was defined "radius of influence" r_i the distance from the axis of symmetry where (see also Fig.14):

$$T_i - T = 0.1\,(T_i - T_c) \qquad (3.6.2)$$

This definition was used to plot the calculated radius of influence versus the experimental value, and the results for a typical test on Macor are presented in Fig.15.

The above mentioned inadequacy of the concept of contact temperature affects also the definition of the radius of influence, but this is more evident when the solid surface consists of a material with very high thermal conductivity. In fact, the distribution of temperature in the experiments on Macor is always

characterized by sharp differences between the values under the droplet and the values on the exposed surface, and also by strong gradients dT/dr on the exposed surface: with this configuration, any reference temperature is apparently acceptable in order to individuate an area influenced by the cooling effect of the impinged droplet. This is not acceptable, of course, from the point of view of the physical meaning. Moreover, the same method becomes highly inaccurate when one tries to apply it to solid surfaces like aluminum, since the differences of temperature and the radial gradients, in those cases, are far below the minimum experimental error (Δt=0.1-0.5 °C versus exp.error=1.0-2.0 °C). To find a correlation between a radius of influence and a meaningful physical parameter, it was eventually decided to use the fluxes in lieu of the temperatures. Since it is:

$$\frac{\rho V h_{fg}}{A_w \tau} = k \frac{1}{R} \frac{\partial T}{\partial r} \qquad (3.6.3)$$

where A_w is the wetted area, it is also possible to find the points where, for example:

$$0.01 \frac{\rho V h_{fg} R}{A_w \tau k} = \frac{\partial T}{\partial r} \qquad (3.6.4)$$

On this conceptual basis, a new definition of the radius of influence is currently being developed. The use of heat fluxes instead of temperatures as reference parameters is expected to be much more effective to obtain a more general description of the cooling effect of the droplet on various materials.

A simplified model for droplets evaporating on high conductivity solids was based on the assumption of uniform and constant temperature under the droplet and on the dominance of the axial component of the flux over its radial component in the liquid droplet. The results for Macor, however, show that the assumptions of the simplified model cannot be applied to low conductivity solids since the solid-liquid interfacial temperature is neither constant nor uniform throughout the evaporation process. In Fig.16 the solid-liquid interfacial temperature is shown for different times and locations under the droplet. The results presented refer to a 30 μl droplet which, deposited both on aluminum and Macor, generated the same calculated contact temperature of 82 °C. It is clear that the hypothesis of uniform and constant temperature at the solid-liquid interface is acceptable for aluminum but not for Macor.

As it was previously anticipated, the assumption of one dimensional heat flux in the droplet axial direction (normal to the solid surface) can be considered quite accurate (already shown in Fig.12).

A set of plots obtained with the current version of the code is presented in Figs.17-20. In these figures the surface temperature distributions and the interfacial heat fluxes for aluminum and Macor are shown. They constitute the most recent and reliable numerical results obtainable with the coupled model described in this report.

4. CONCLUSION AND FUTURE WORK

4.1 Remarks

The coupled model which was obtained in the last year of researches can be seen both as a basic result and as a turning point in the numerical part of this work. Even if some characteristics of the code have still to be improved or modified, the numerical predictions concerning the evaporation time and the temperature distributions are reliable and can be used for a broad range of materials constituting the solid hot surface.

With the new definition of the radius of influence, also the cooling effect of the droplet will be known in detail regardless of the chosen solid surface.

Therefore, all the results obtained in the studies of a single droplet behavior are ready to be averaged and used to analyze the evaporation of a more complicated system, consisting of a larger number of droplets randomly impinging on a defined portion of a hot solid surface. The experimental and theoretical programs related to this subjects will constitute the main work of next grant period, together with the work that is still required to improve the accuracy and the generality of the already existing numerical code. These programs of future work are described in the following paragraphs.

4.2 Experimental and Analytical Programs

The coupled solution for the low thermal conductivity solid case will be improved and compared with experimental measurements of the solid surface temperature via infrared thermography. A new set of experiments on a quartz semi-infinite solid are under way and initial efforts to set-up the infrared thermography apparatus have been made. Another area of research that will be developed in the next grant period is involved with the generation of small droplets (order of one microliter). These droplet are in the same size range of those generated by commercial sprinklers.

The solids analyzed in this initial portion of the research program are heated from below by an electrical hot plate. In the actual fire application the heat is transmitted to the water droplet and to the surface by radiation from above. The new experimental set-up where both the droplet and the surface will receive radiative heat from gas fired panels will be the main experimental apparatus in the next grant period. A solid block with embedded thermocouples will also be tested in this radiant heat set-up to validate the modelling of the solid thermal behavior for internal points.

The experimental program on radiative heating will be conducted in parallel with the development of a modified numerical code; this will take into consideration the radiative contribution as a new boundary condition replacing the conductive one.

At the same time, the results of the experimental and numerical work done will be newly used in order to provide a more extensive model which will analyze a multi-droplet evaporative transient. The data obtained for the single droplet will be averaged and applied to the more complex situation that has to be considered when a hot solid surface is wetted under the action of a multi-droplet dispenser. The project and the experimental tests concerning that dispenser are already in progress.

5. ACKNOWLEDGEMENTS

The authors wish to acknowledge the precious guidance of Dr. H. Baum of the Center for Fire Research which was essential for the derivation of the boundary element method. The Computer Science Center of the University of Maryland provided funding for the computational expenditures.

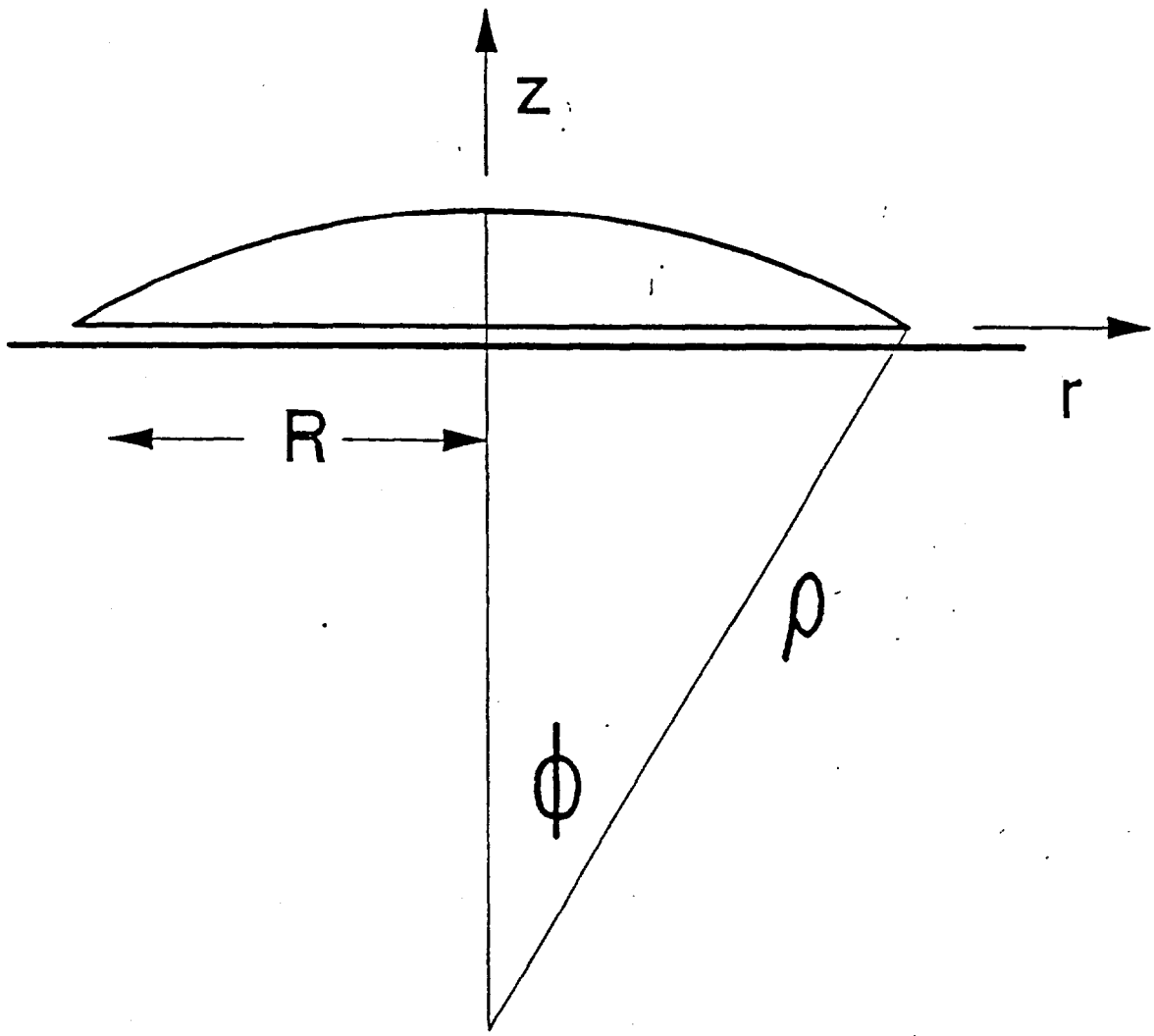

Fig.1 System geometry and coordinates

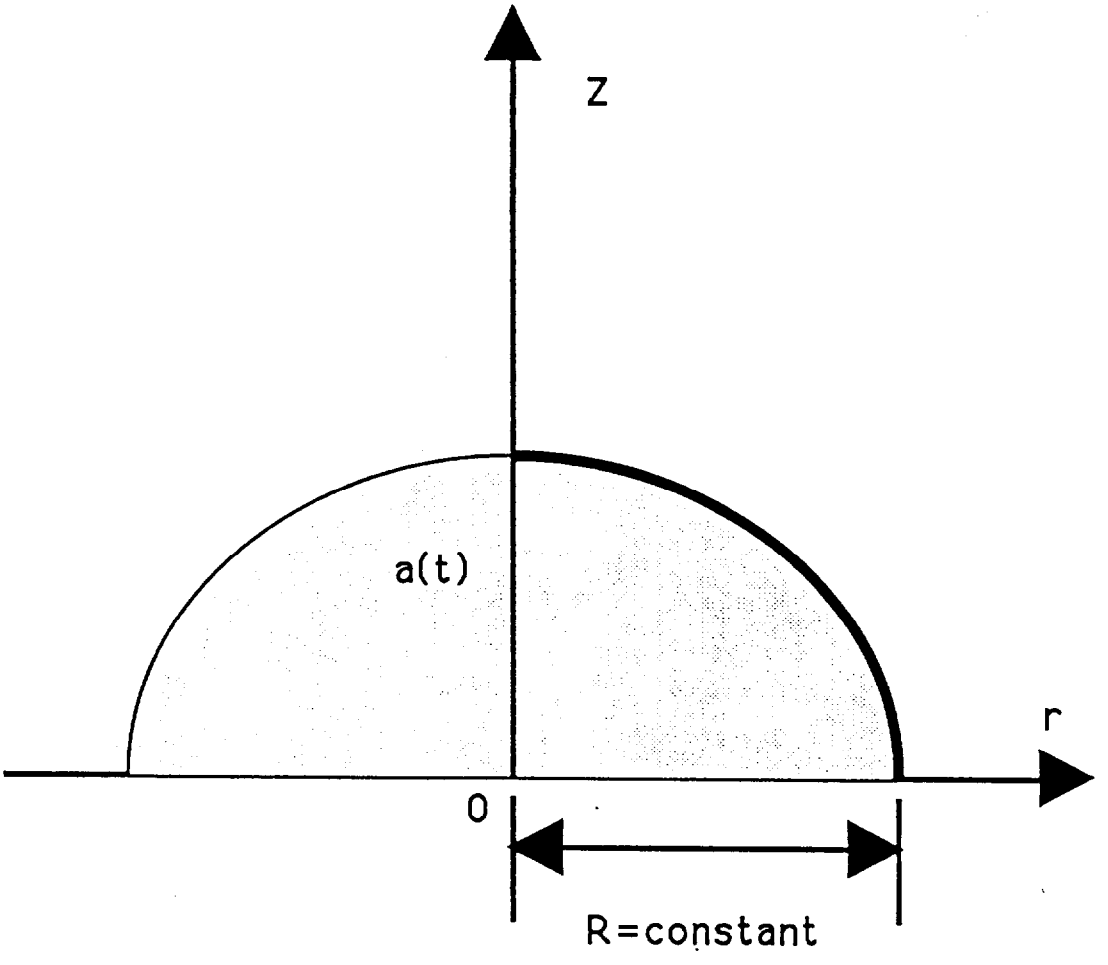

Fig.2 Shape of the droplet (spherical segment)

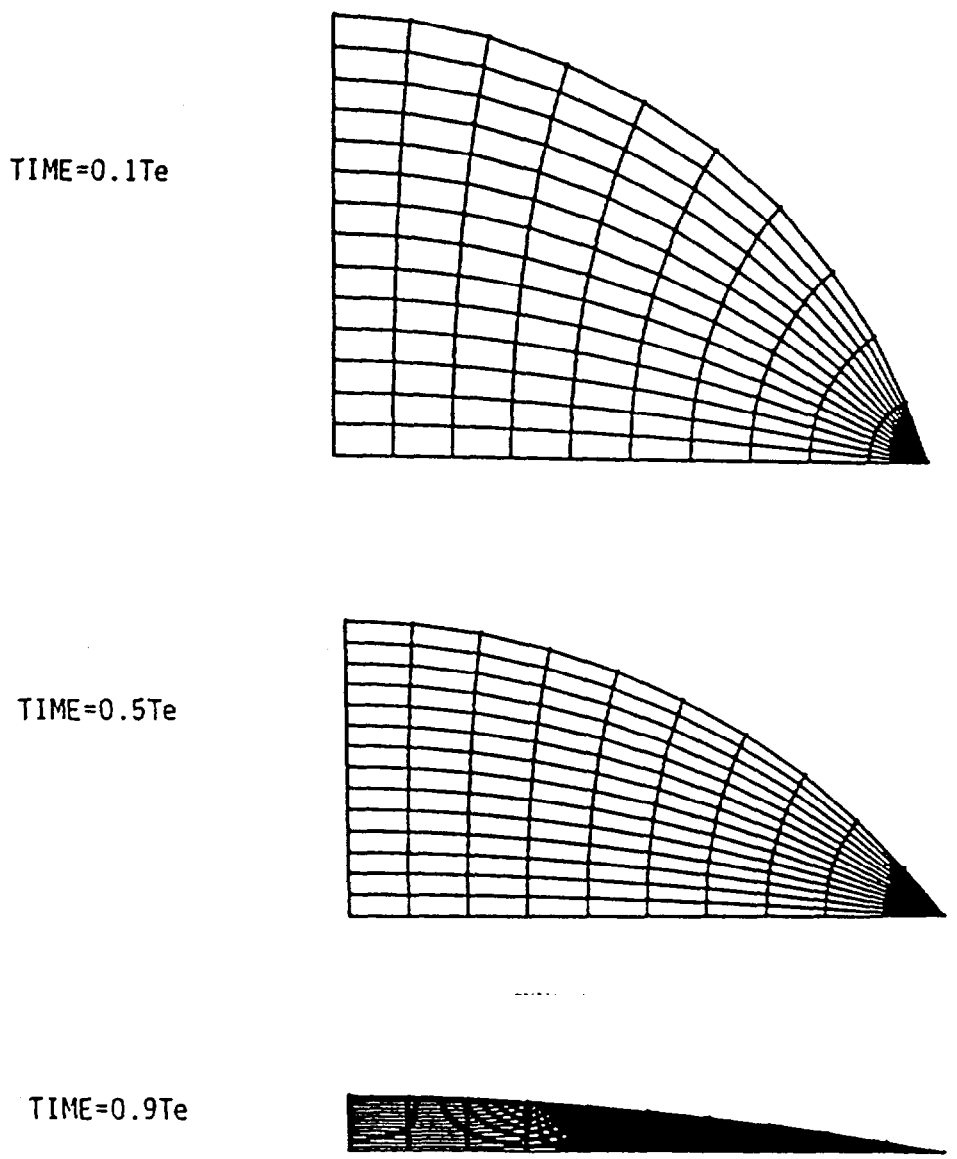

Fig.3 Droplet nodalization: temporal behavior

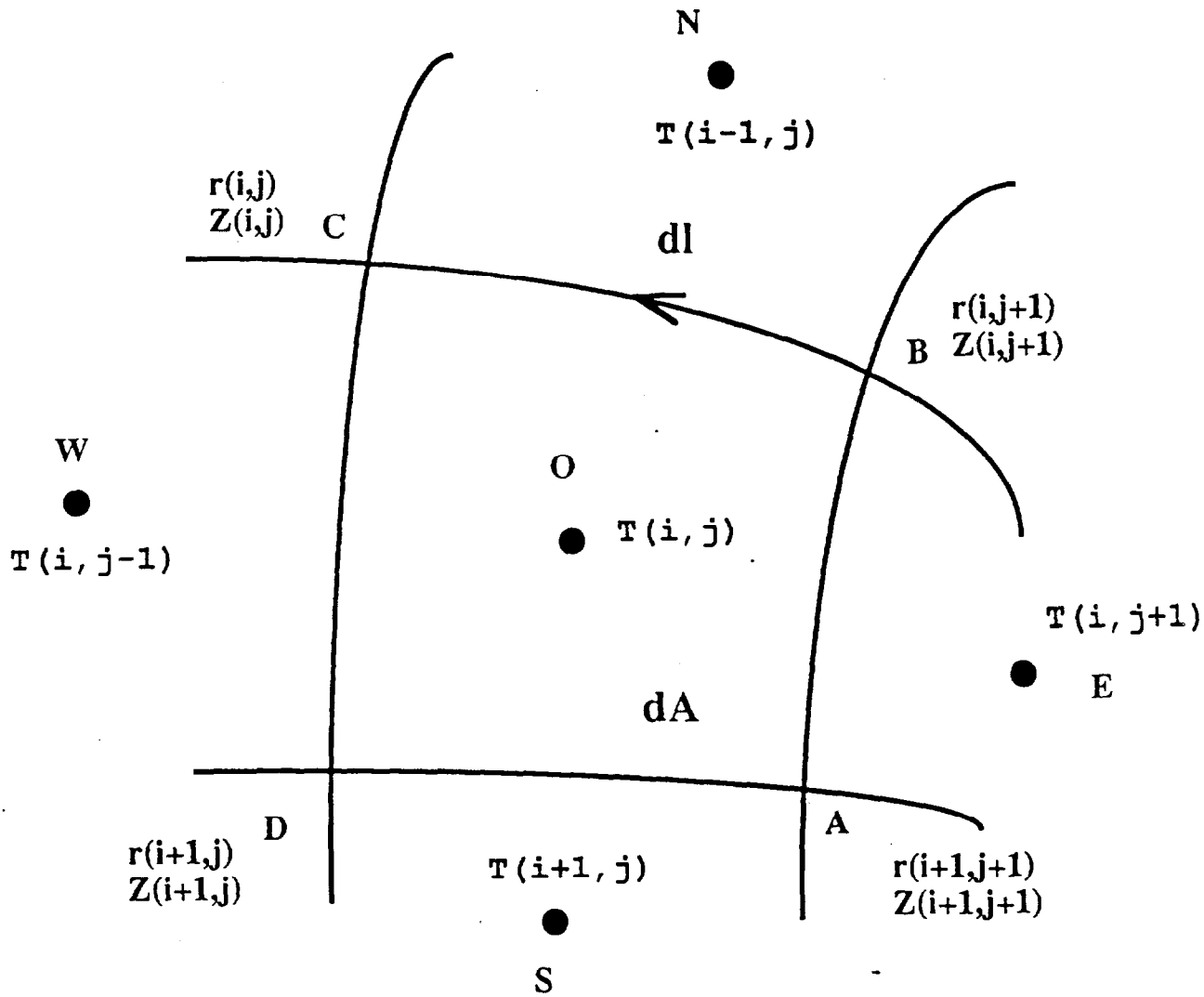

Fig.4 Control volume nodalization: center field

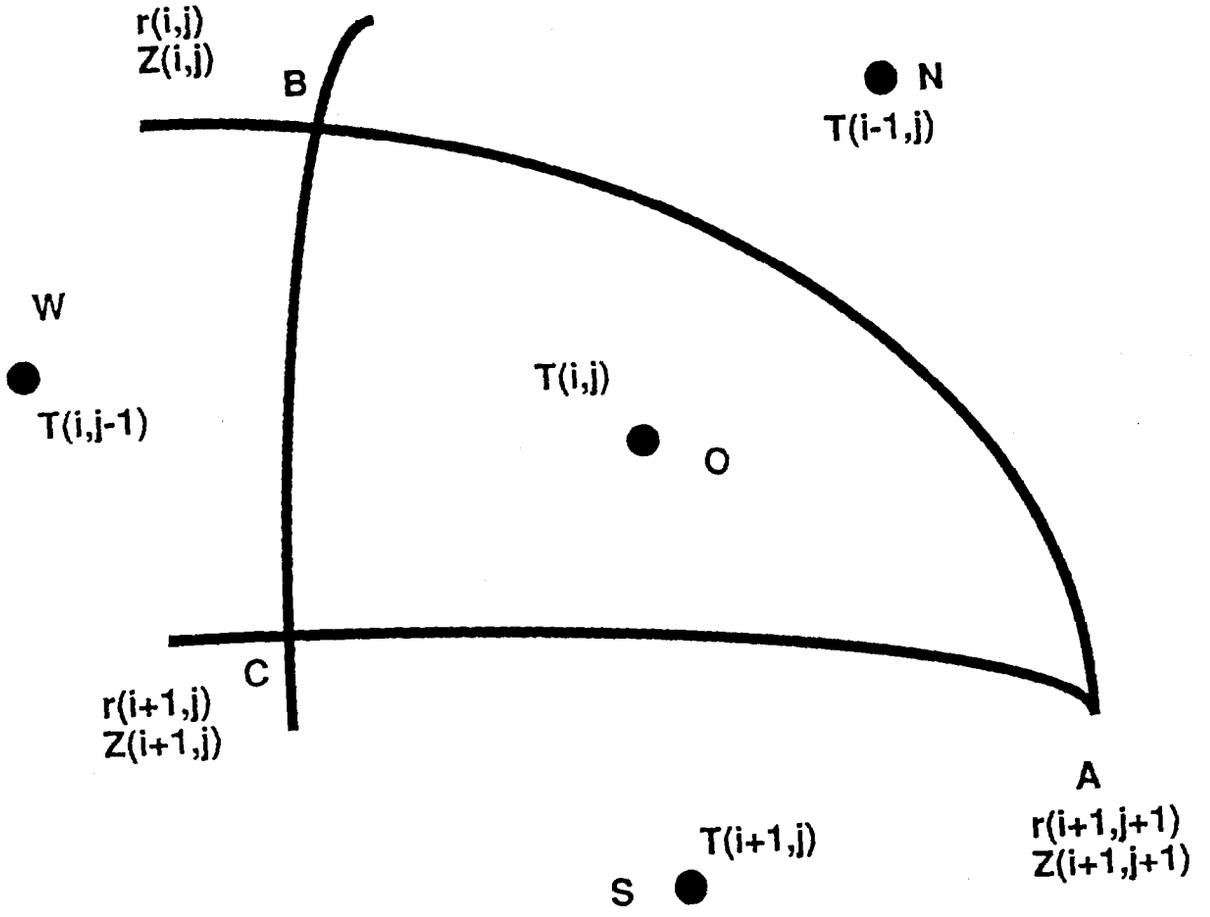

Fig.5 Control volume nodalization: edge of the droplet

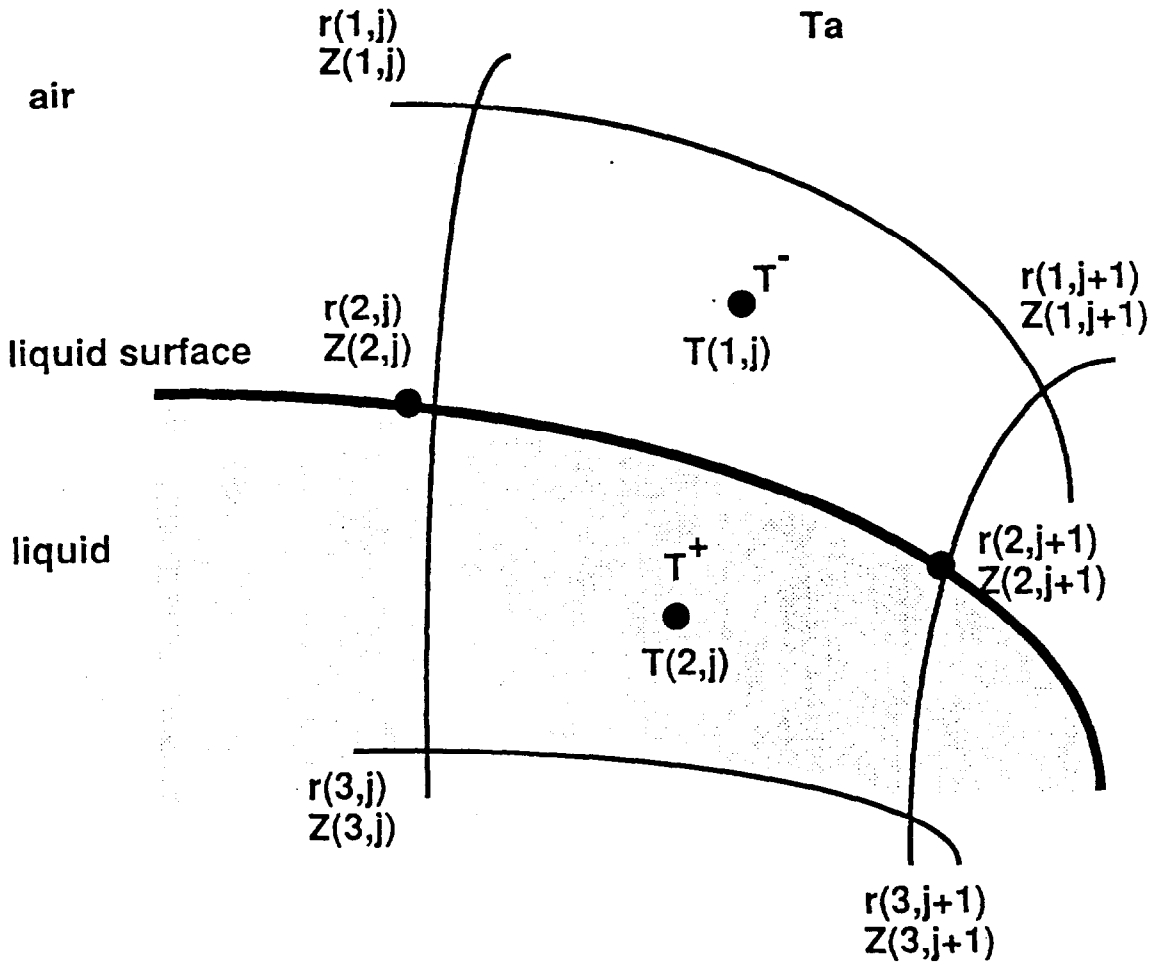

Fig.6 Control volume nodalization: liquid-ambient interface

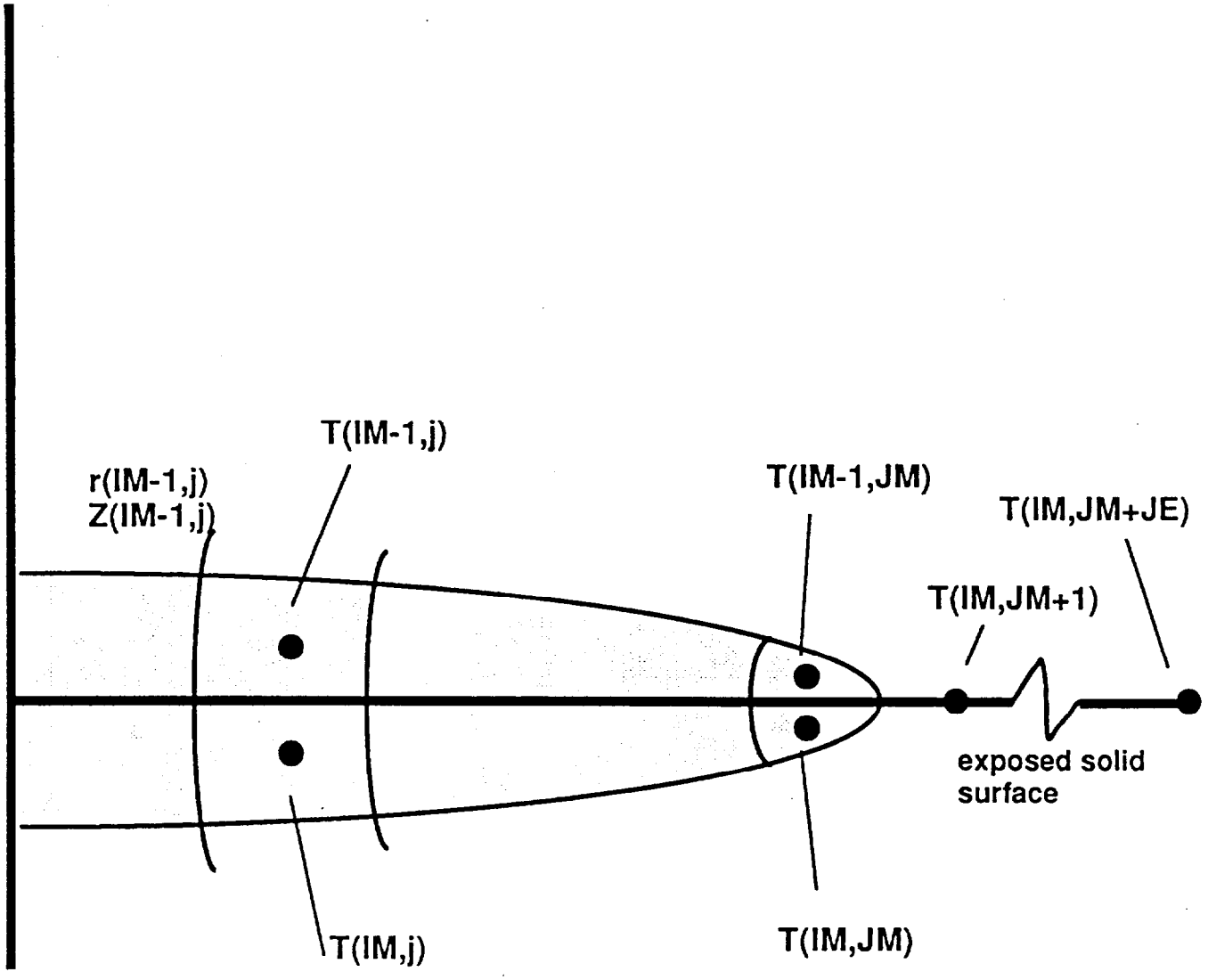

Fig.7 Coupled model: liquid-solid interface

Matrix B:

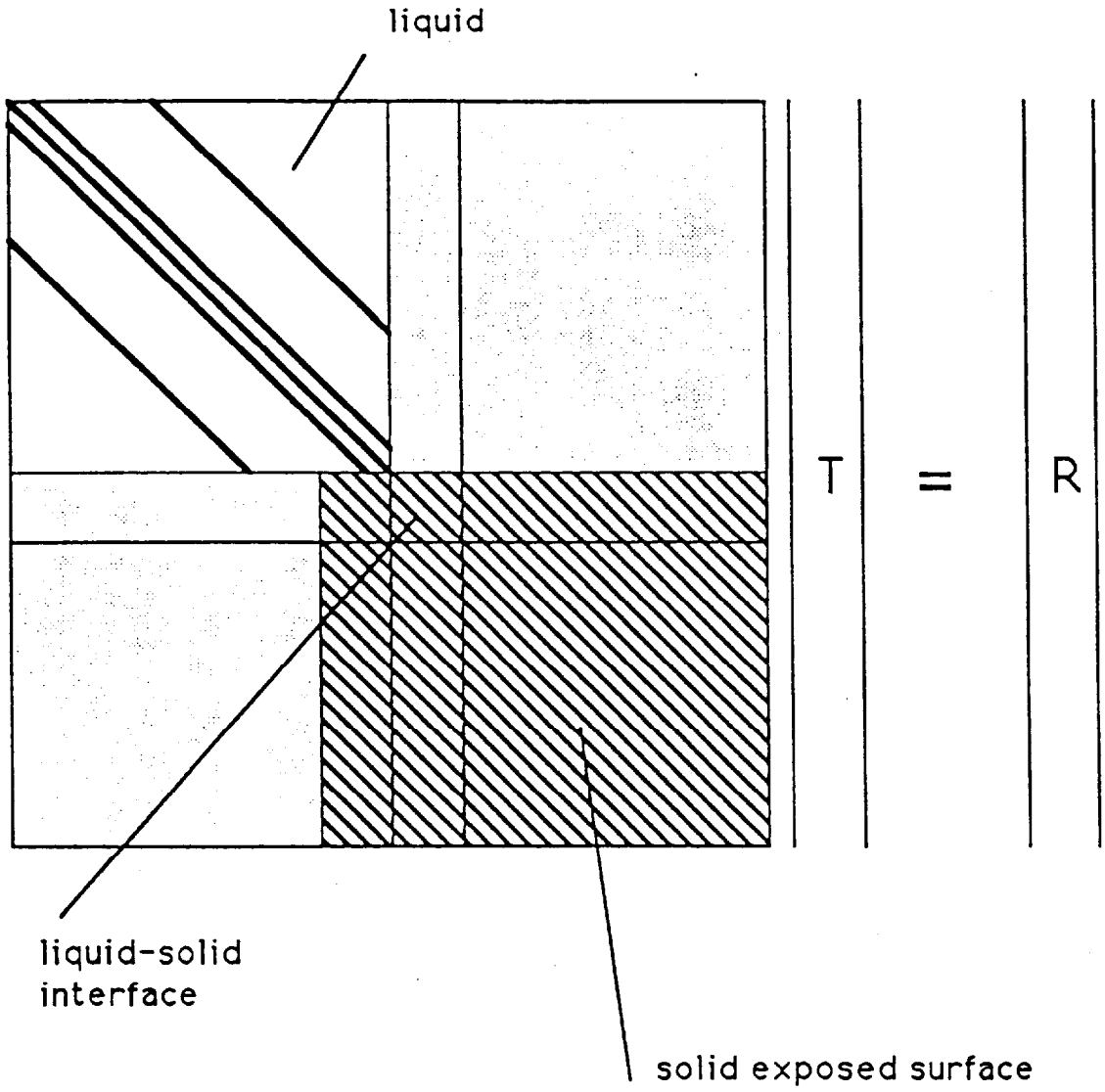

$$B \bullet T = R$$

Fig.8 Shape of the matrix of coefficients

Flow Chart:

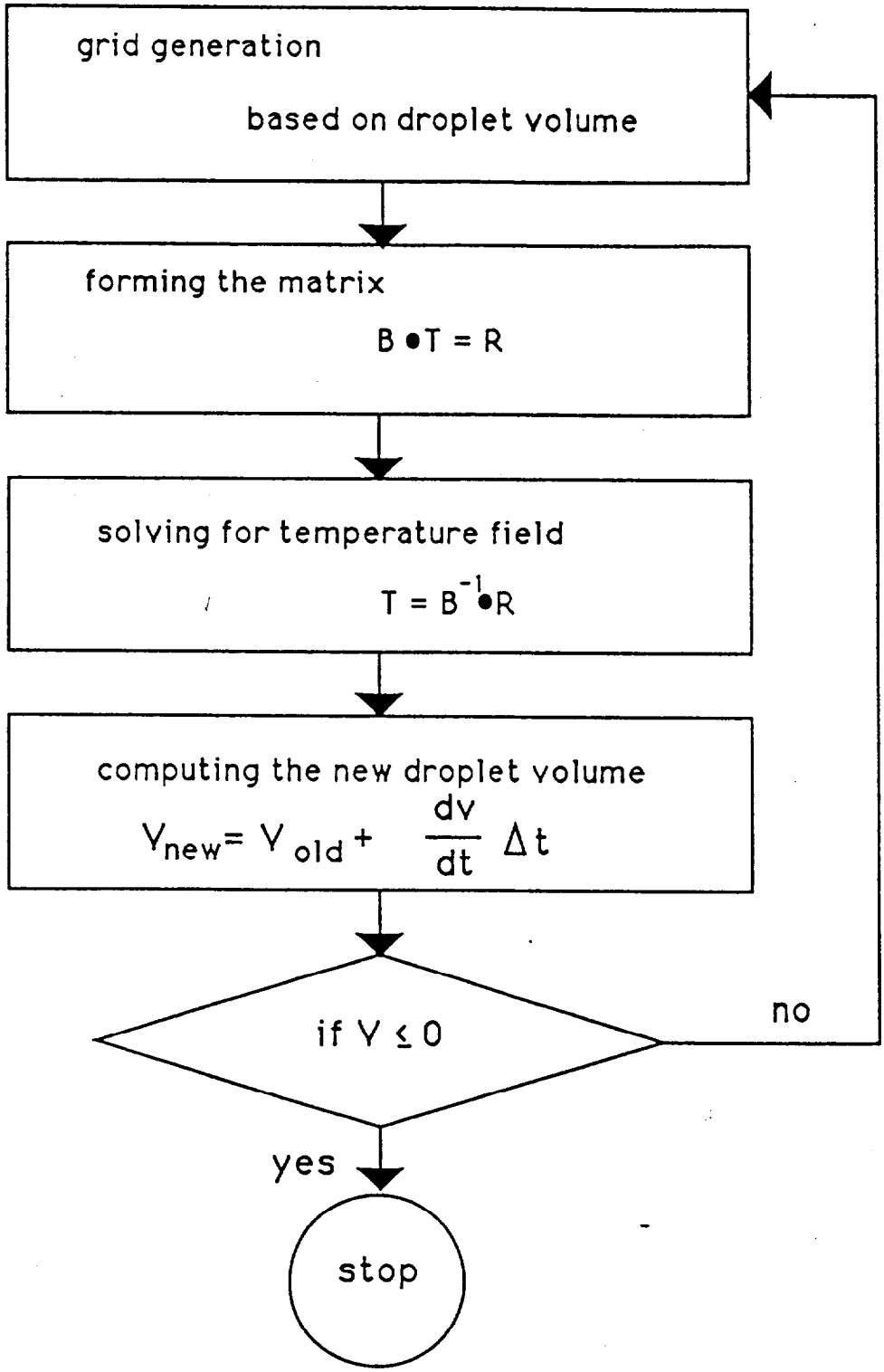

Fig.9 Flow chart of the liquid nodalization

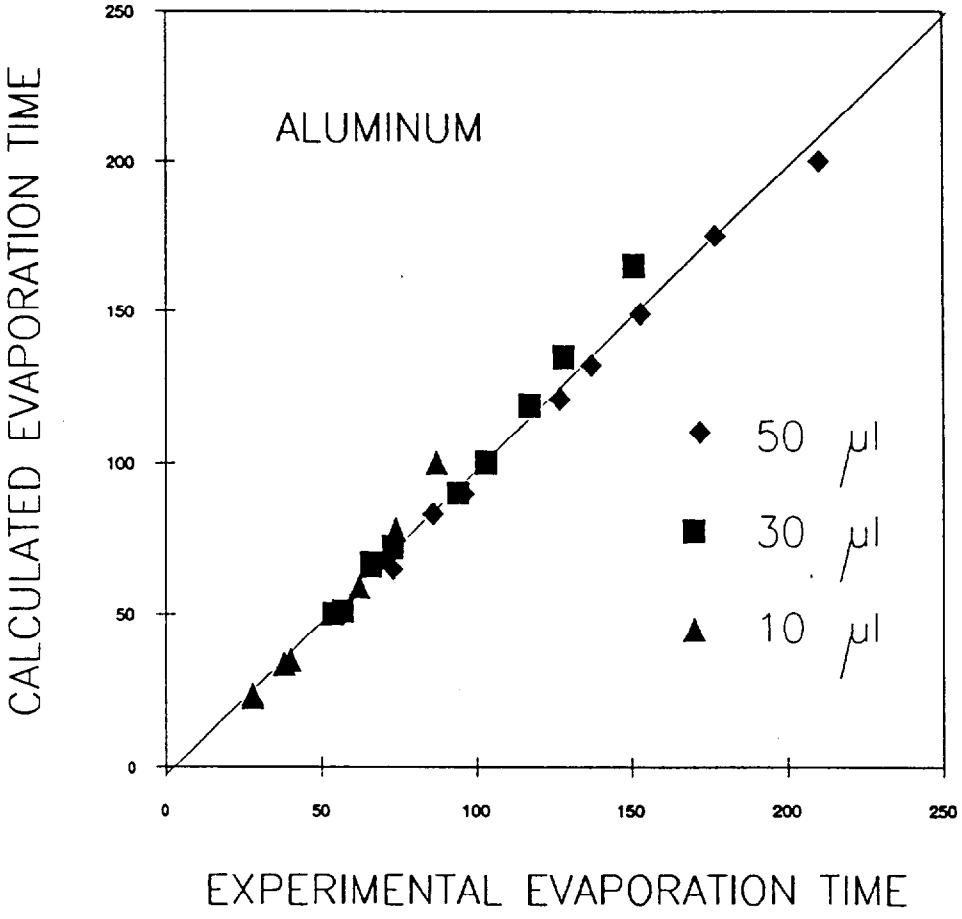

Fig.10 Evaporation time on aluminum: computations versus measurements

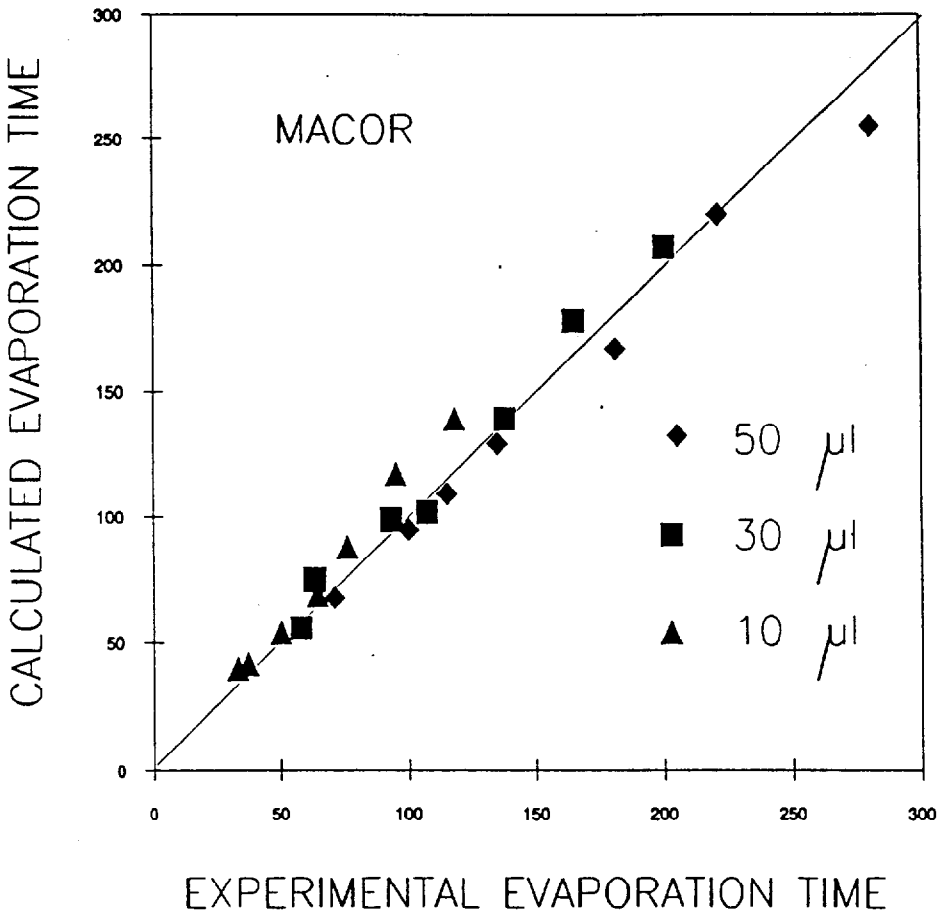

Fig.11 Evaporation time on Macor: computations versus measurements

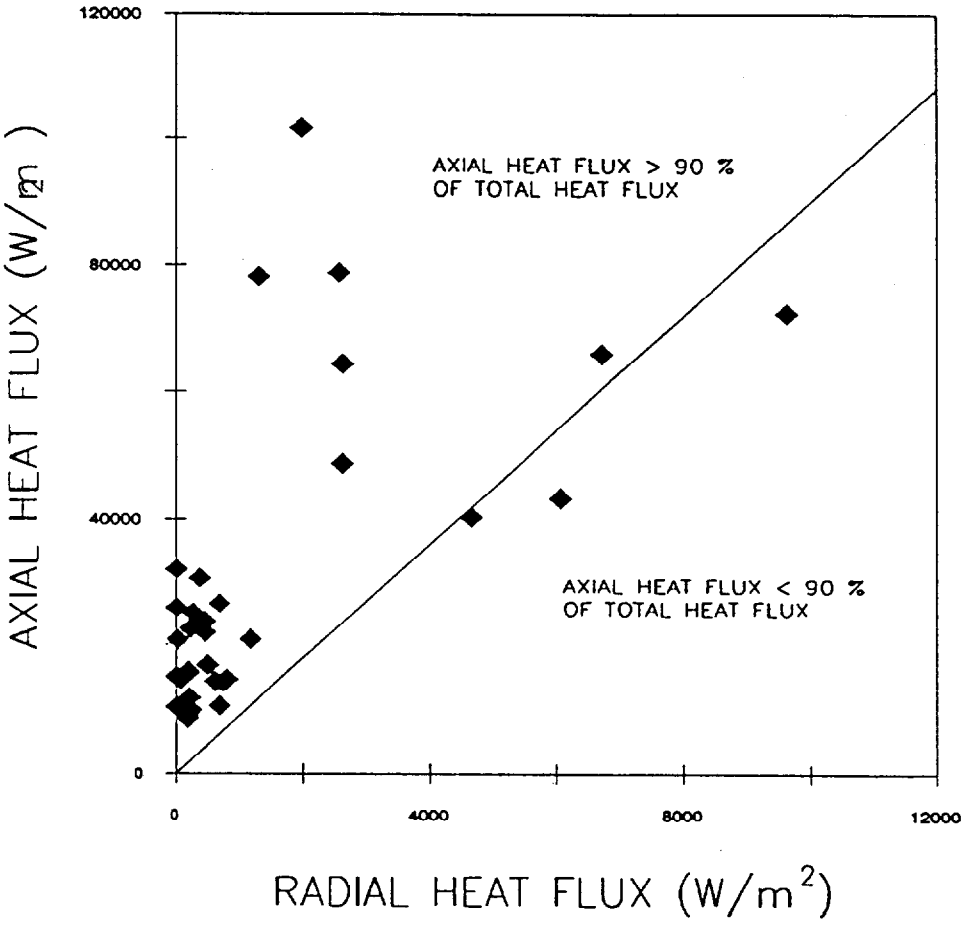

Fig.12 Axial and radial heat flux components: validation of the simplified thermal conductivity model assumptions

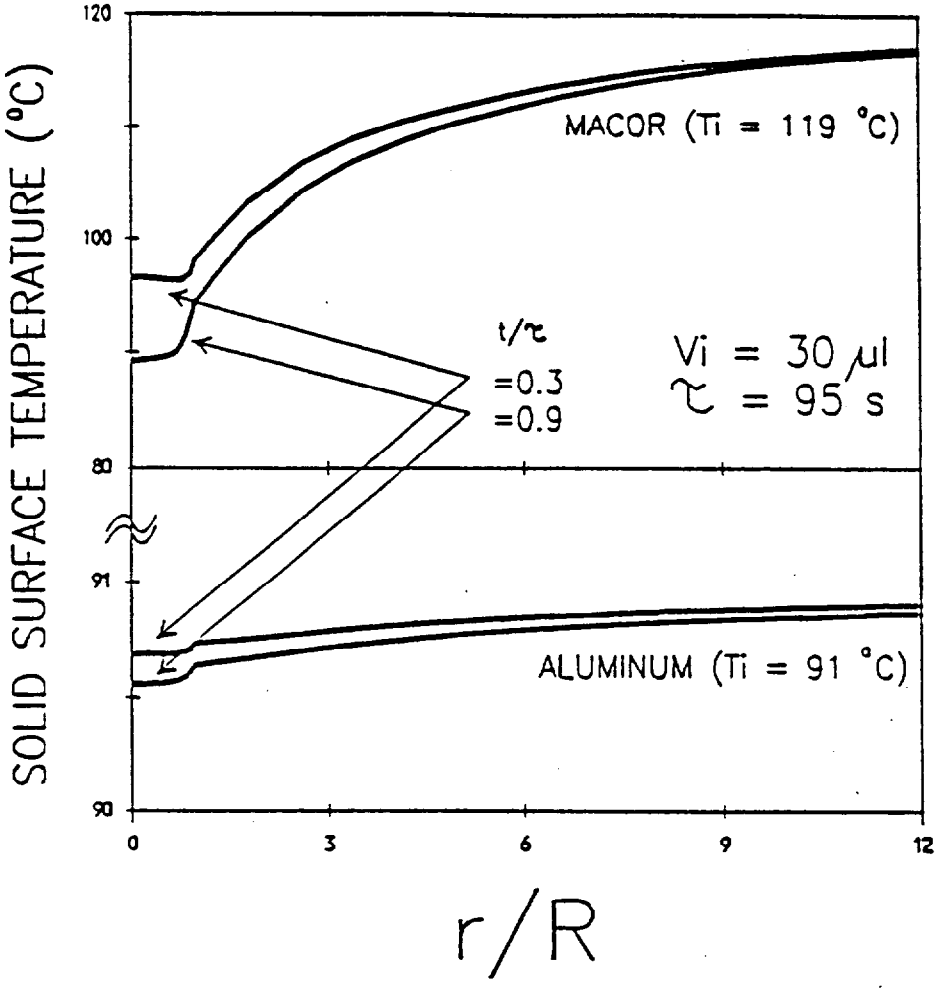

Fig.13 Solid surface temperature profiles for droplets on Macor and aluminum with identical calculated contact temperature

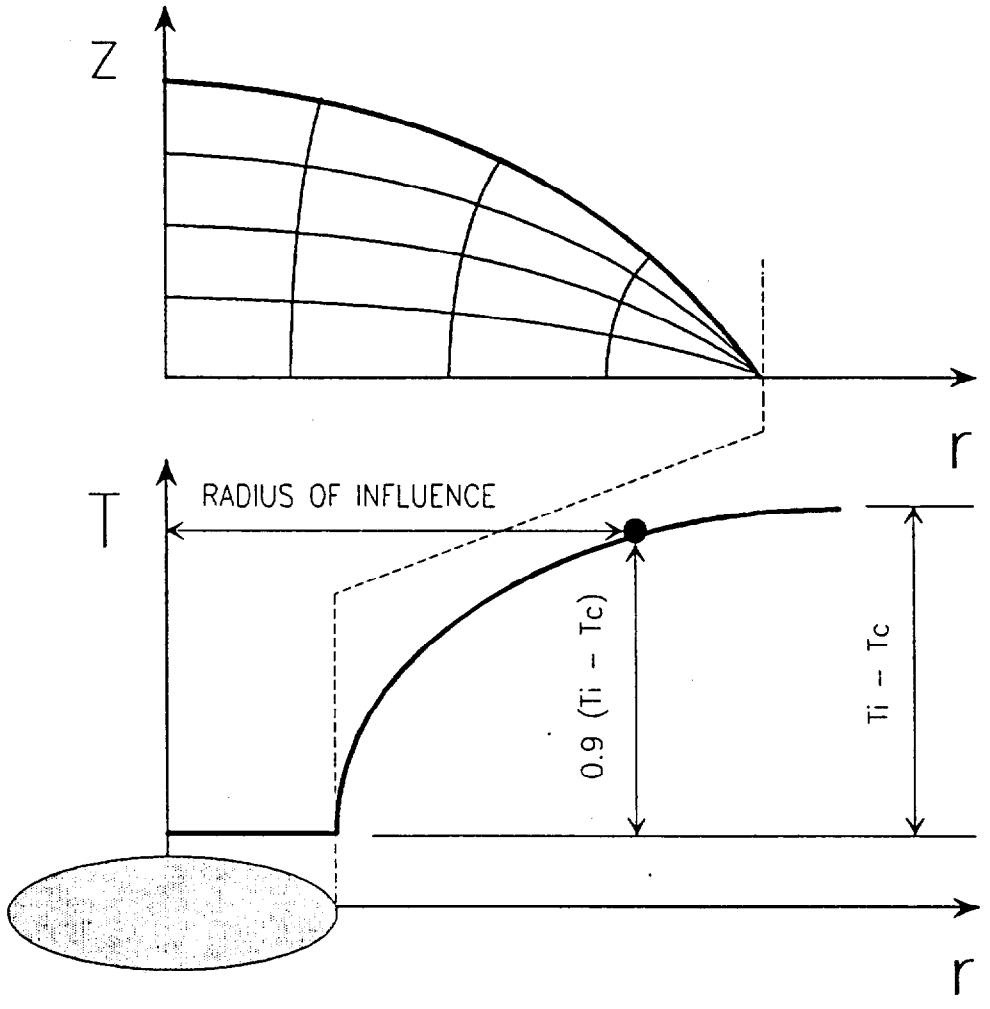

Fig.14 Radius of influence

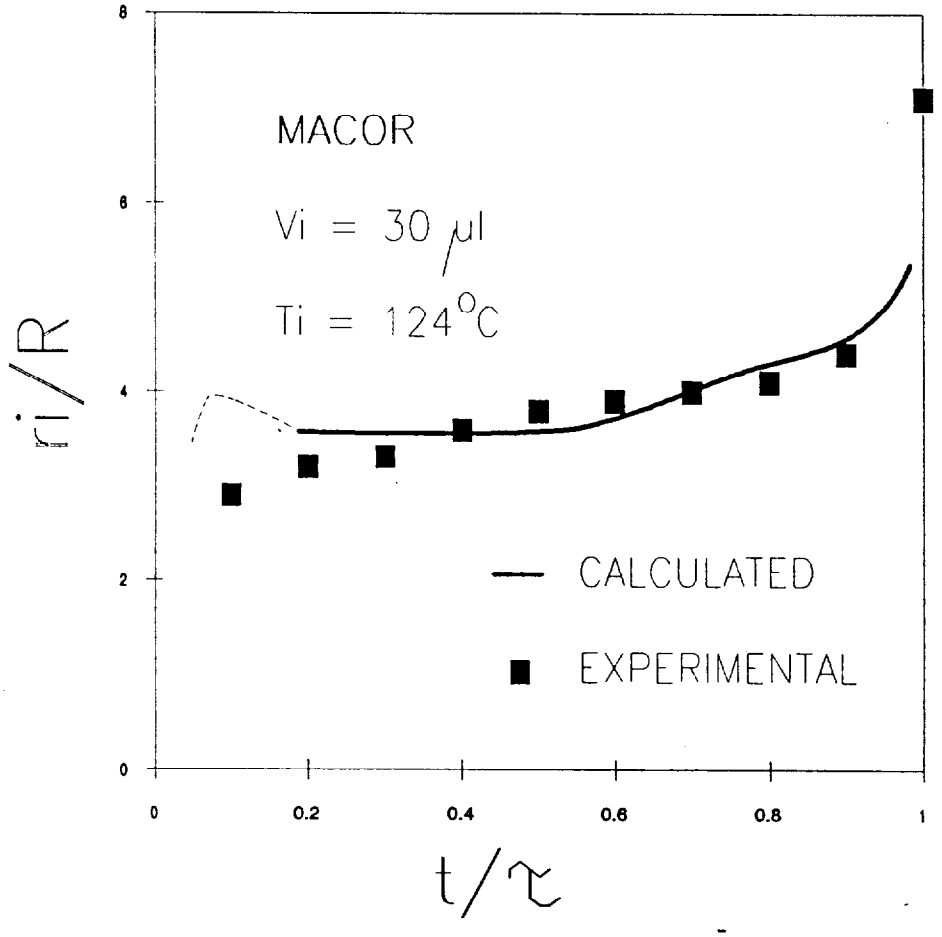

Fig.15 Radius of influence versus time: computations versus measurements

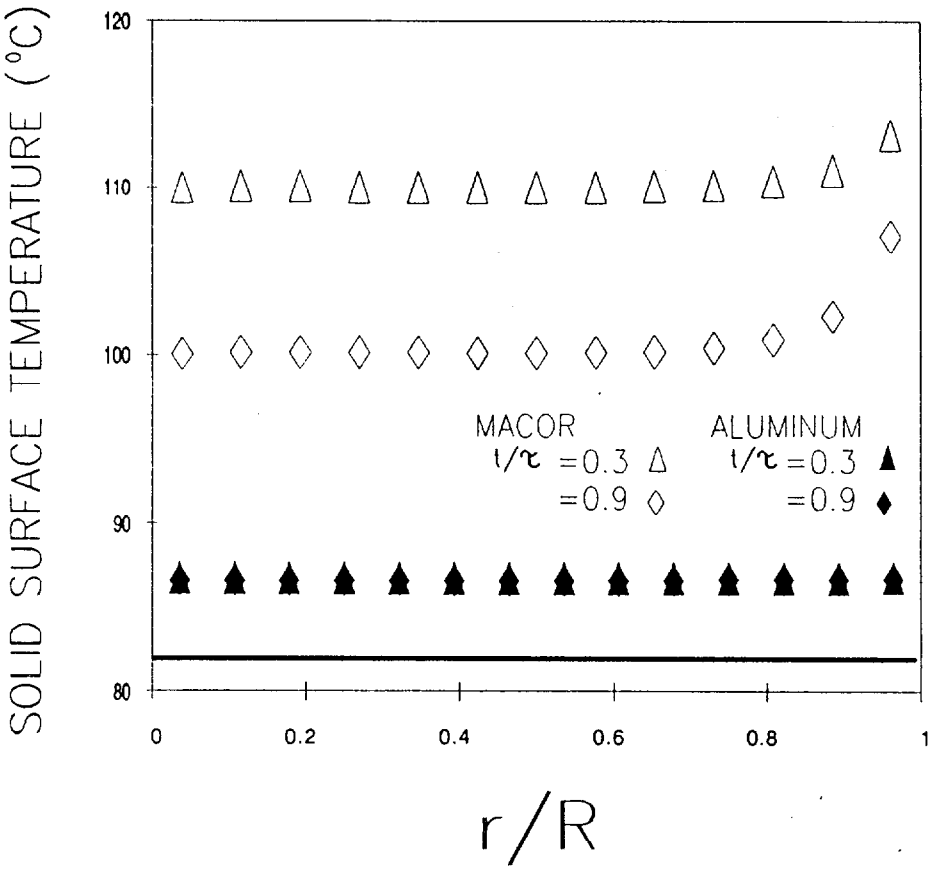

Fig.16 Solid-liquid interfacial temperature: simplified high thermal conductivity model assumptions

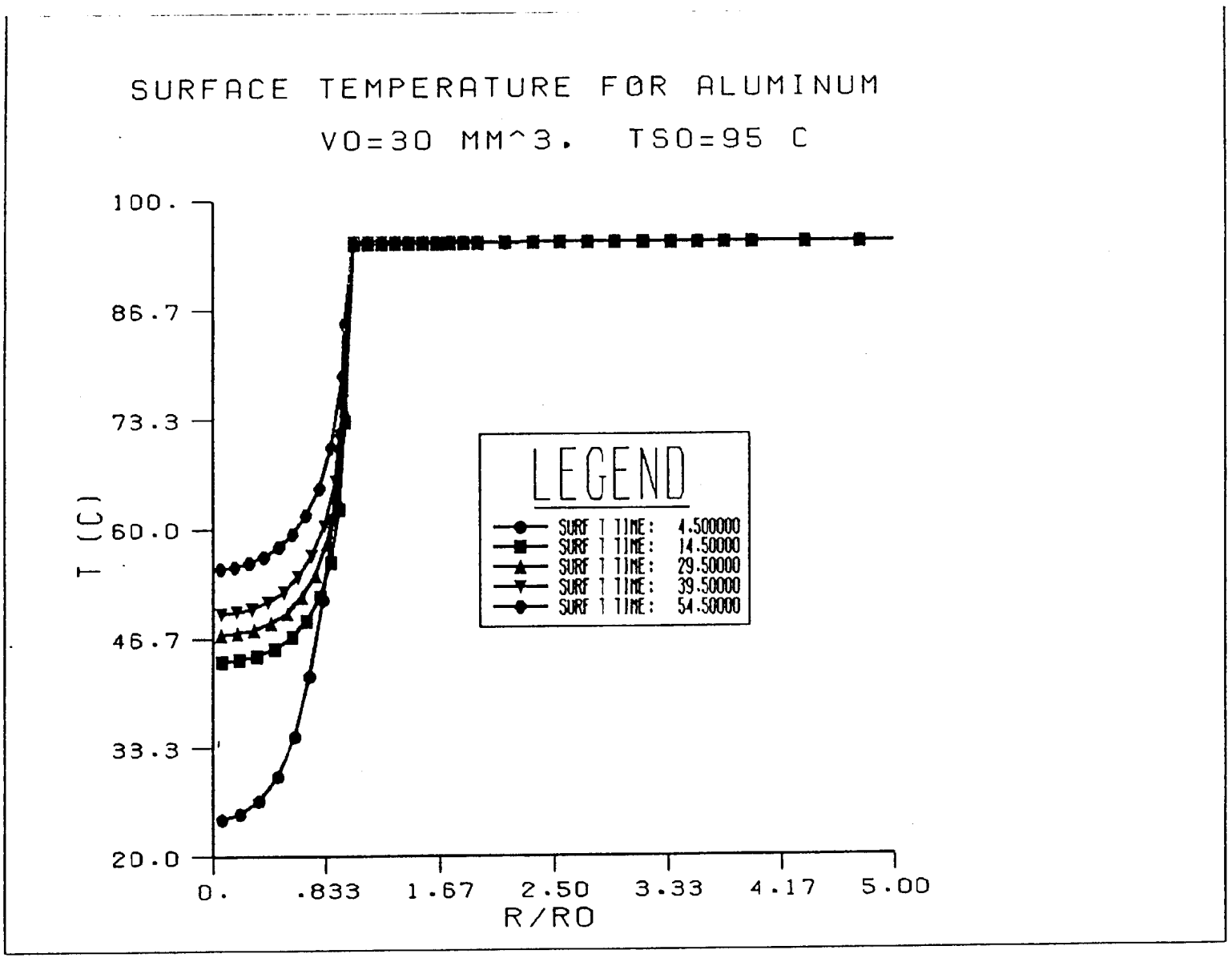

Fig.17 Solid surface temperature profiles for Aluminum during the evaporative transient

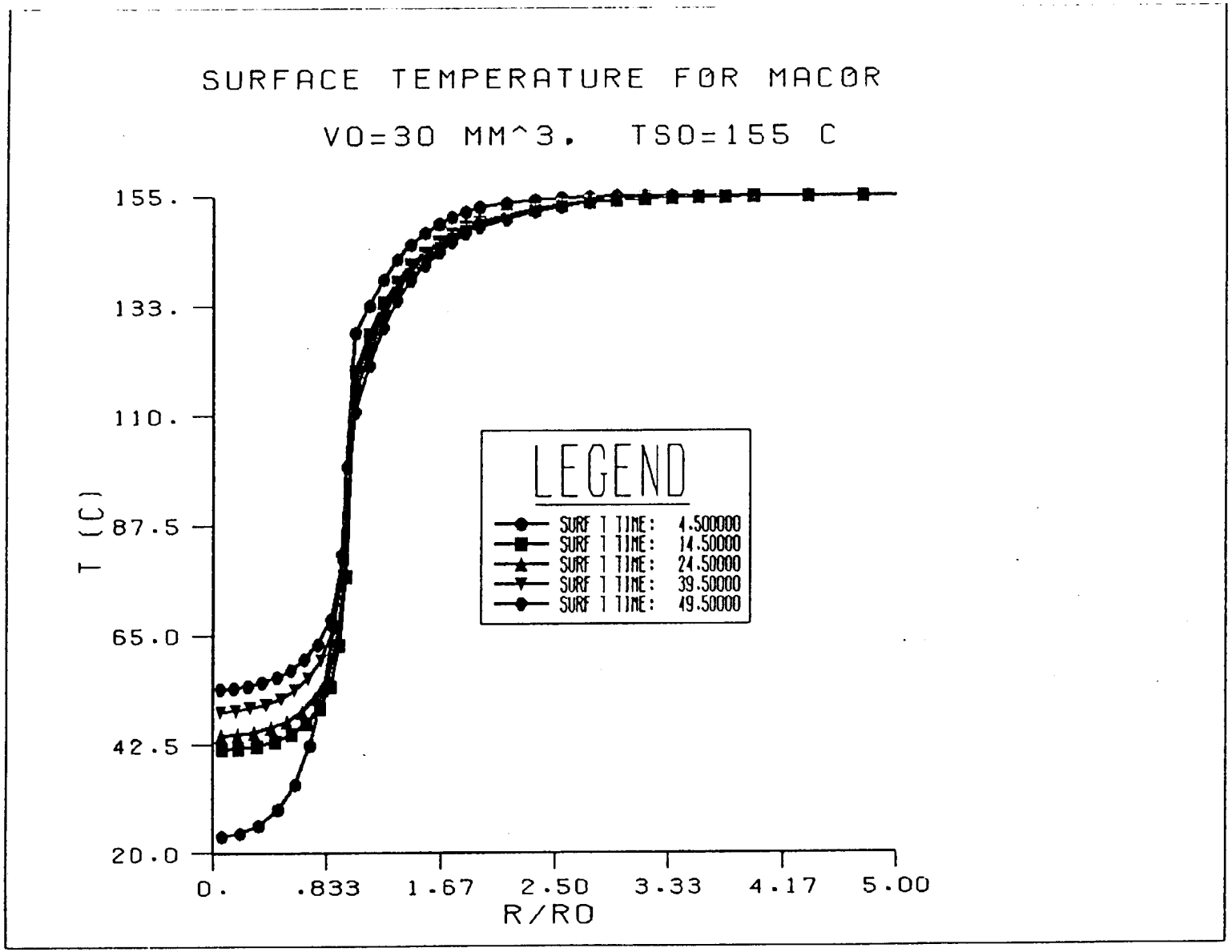

Fig.18 Solid surface temperature profiles for Macor during the evaporative transient

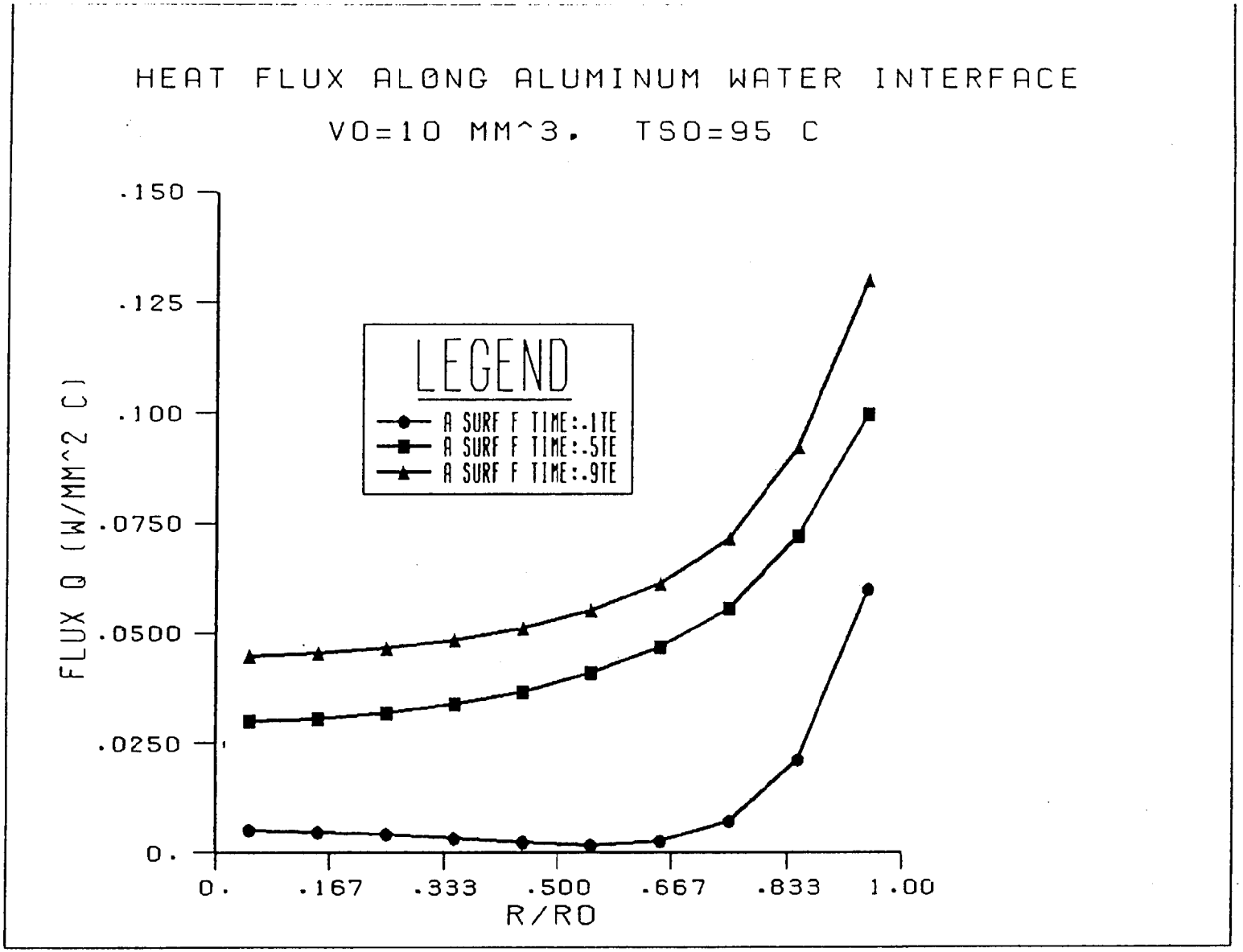

Fig.19 Heat flux along aluminum-water interface

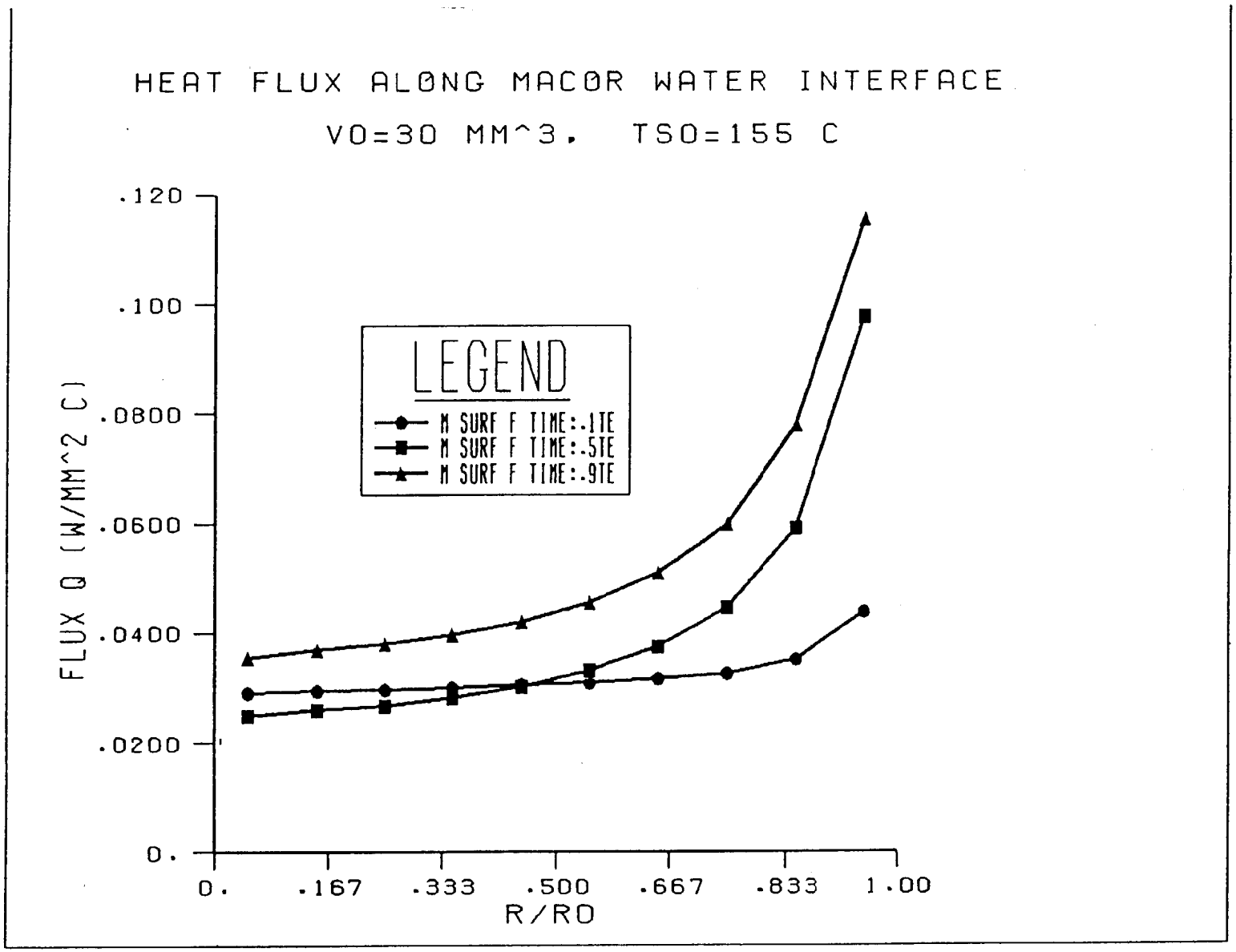

Fig.20 Heat flux along Macor-water interface

7. APPENDIX

```
C......PROGRAM FOR SOLVING A CONDUCTION HEAT TRANSFER PROBLEM IN A LIQUID
C......DROPLET LAID ON THE SURFACE OF AN INFINITE LARGE SOLID.
C......THE INTEGRATED CONTROL VOLUME METHOD IS USED IN THIS TRANSIENT
C......PROBLEM.
C......CRANK-NICHOLSON SCHEME IS USED
       PARAMETER (IM=16,JM=11,JS=JM-1,JE=4*JS,KNT=10,NIMSL=IM*JM+JE)
       DIMENSION TN1(IM*JM+JE),TR(IM*JM+JE)
       DIMENSION TX(IM*JM+JE),TA(IM*JM,4),TB(IM*JM+JE,IM*JM+JE)
       DIMENSION W(JM+JE-1,JM+JE-1),FTIM(JM+JE-1,KNT),F(JM+JE-1)
       DIMENSION RHS(JM+JE-1),CT(JM),W0(JM+JE-1,JM+JE-1)
       DIMENSION EWIS(JM),SX(JM),SX2(JM)
       DIMENSION R(IM+1,JM+1),Z(IM+1,JM+1),DZ(JM),RS0(JM+JE)
       DIMENSION RO3(IM),ZO3(IM),NPTT(50)
       DIMENSION IWK(NIMSL),WK(NIMSL+NIMSL*(NIMSL-1)/2)
         COMMON /CONST/ ALFA,PI
         COMMON /GRID/ DR0,DT0,NDP,NP,TN
         COMMON /INTG/ AT0,ERRREL,IRULE
         COMMON /SOLID/ SK,SC,SR
         COMMON /WATER/ COEFKW,CPW,RHOW
         PI=4.*ATAN(1.0)
         IRULE=2
         AT0=0.001
         ERRREL=0.001
         NTCI=1
         NTCS=1
         DTIME=1.
         NTIME=500
         READ(5,*)VO
         READ(5,*)BETA
         RR=BETA*EXP(1./3.*LOG(.75*VO/PI))
         UU=EXP(1./3.*LOG(3.*VO/PI+SQRT(RR**6+9./PI**2*VO**2)))
         AA=UU-RR**2/UU
C...AIR TEMP.
       TMPAIR=20.
C...INITIAL TEMPERATURE OF THE LIQUID DROP
       TEMP0=20.
C...INITIAL TEMPERATURE OF THE SOLID
       READ(5,*)TSLD0
C...ALL TEMPERATURES USED HERE, TN1 AND TX, ARE DELTAT : U=TEMP-TMPAIR
       TAIR=TMPAIR-TMPAIR
C...SOLID CONDUCTIVITY (SK:W/MM K; SR:KG/MM^3; SC:J/KG K)
        SK=180.E-3
        SR=2771.E-9
        SC=962.32
        RHK=SH/SK
C...DIFFUSIVITY OF SOLID (MM^2/S)
        ALFA=SK/(SR*SC)
C...WATER DENSITY (KG/MM^3)
       RHOW=997.6E-9
C...WATER CONDUCTIVITY (W/MM K)
       COEFKW=.613E-3
C...WATER SPECIFIC HEAT(J/KG K)
      CPW=4179.
C...DIFFUSIVITY OF WATER: ALPHA=KW/(RHO*CP) (MM^2/S)
        ALPHA=COEFKW/(RHOW*CPW)
C...AIR SPECIFIC HEAT (J/KG K)
       CA=1009.
C...AIR PRESSURE (BAR)
       PA=1.014
C....CONTACT TEMPERATURE
```

```
      CALL CTEMP0(IM,JM,JE,TMPAIR,TN1,TSLD0,CT)
C.....
      CALL RSD(JM,JS,RR,RS0)
       TTT=.5
       NDP=JM-1
       NP=JM+JE-1
       TN=KNT
       DT0=DTIME
       DR0=RR/(1.*JM-1.)
C.....
      CALL WEIGHT(TTT,W0,RS0)
C.....
       DO 1 NT=1,NTIME
C.....
      TIME=NT*DTIME-.5*DTIME
C...SET NEW GRID POINTS BASED ON NEW RR,AA
      CALL RZ90(IM,JM,RR,AA,R,Z)
      CALL TRI0(IM,JM,R,Z,RO3,ZO3)
      CALL DZ0(IM,JM,R,Z,RO3,ZO3,DZ)
C...
      DO 90 I=1,IM*JM+JE
      DO 90 J=1,IM*JM+JE
      TB(I,J)=0.
 90       CONTINUE
      DO 100 I=2,IM-1
      DO 100 J=2,JM-1
      CALL NEWSO(4,IM,JM,R,Z,RO3,ZO3,
     $           I,J,RN,ZN,RE,ZE,RW,ZW,RS,ZS,RO,ZO)
      ALAB=SQRT((R(I+1,J+1)-R(I,J+1))**2+(Z(I+1,J+1)-Z(I,J+1))**2)
      ALBC=SQRT((R(I,J+1)-R(I,J))**2+(Z(I,J+1)-Z(I,J))**2)
      ALCD=SQRT((R(I,J)-R(I+1,J))**2+(Z(I,J)-Z(I+1,J))**2)
      ALDA=SQRT((R(I+1,J)-R(I+1,J+1))**2+(Z(I+1,J)-Z(I+1,J+1))**2)
      AREA=.25*(ALAB+ALCD)*(ALBC+ALDA)
      DXN=SQRT((RN-RO)**2+(ZN-ZO)**2)
      DXW=-SQRT((RO-RW)**2+(ZO-ZW)**2)
      DXS=-SQRT((RO-RS)**2+(ZO-ZS)**2)
      DXE=SQRT((RE-RO)**2+(ZE-ZO)**2)
      IJ=(I-1)*JM+J
C....
      CONST=.25*DTIME*ALPHA/(RO*AREA)
      AIM1J=CONST*ALBC*(R(I,J+1)+R(I,J))/DXN
      AIJP1=CONST*ALAB*(R(I+1,J+1)+R(I,J+1))/DXE
      AIJM1=-CONST*ALCD*(R(I,J)+R(I+1,J))/DXW
      AIP1J=-CONST*ALDA*(R(I+1,J)+R(I+1,J+1))/DXS
      AIJ=-(AIM1J+AIJM1+AIJP1+AIP1J)
C....
      TB(IJ,IJ+1)=-AIJP1
      TB(IJ,IJ+JM)=-AIP1J
      TB(IJ,IJ-JM)=-AIM1J
      TB(IJ,IJ-1)=-AIJM1
      TB(IJ,IJ)=1.-AIJ
C...
      IF(NT.EQ.1)THEN
      TA(IJ,1)=AIJP1
      TA(IJ,2)=AIP1J
      TA(IJ,3)=AIM1J
      TA(IJ,4)=AIJM1
      ENDIF
      TR(IJ)=TA(IJ,1)*TN1(IJ+1)+TA(IJ,2)*TN1(IJ+JM)
     $+TA(IJ,3)*TN1(IJ-JM)+TA(IJ,4)*TN1(IJ-1)
```

```
     $+(1.-(TA(IJ,3)+TA(IJ,4)+TA(IJ,1)+TA(IJ,2)))*TN1(IJ)
C..SAVE FOR NEXT TIME STEP
       TA(IJ,1)=AIJP1
       TA(IJ,2)=AIP1J
       TA(IJ,3)=AIM1J
       TA(IJ,4)=AIJM1
  100      CONTINUE
C....FOR J=JM
       J=JM
       DO 110 I=2,IM-1
       CALL NEWSO(3,IM,JM,R,Z,RO3,ZO3,
     $             I,J,RN,ZN,RE,ZE,RW,ZW,RS,ZS,RO,ZO)
       ALCA=SQRT((R(I,J+1)-R(I+1,J))**2+(Z(I,J+1)-Z(I+1,J))**2)
       ALAB=SQRT((R(I,J+1)-R(I,J))**2+(Z(I,J+1)-Z(I,J))**2)
       ALBC=SQRT((R(I+1,J)-R(I,J))**2+(Z(I+1,J)-Z(I,J))**2)
       AREA=.25*(ALCA+ALAB)*(ALBC+ALAA)
       DXN=SQRT((RN-RO)**2+(ZN-ZO)**2)
       DXW=-SQRT((RO-RW)**2+(ZO-ZW)**2)
       DXS=-SQRT((RO-RS)**2+(ZO-ZS)**2)
       IJ=(I-1)*JM+J
C....
       CONST=.25*DTIME*ALPHA/(RO*AREA)
       AIJP1=0.
       AIP1J=-CONST*ALCA*(R(I+1,J)+R(I,J+1))/DXS
       AIM1J=CONST*ALAB*(R(I,J+1)+R(I,J))/DXN
       AIJM1=-CONST*ALBC*(R(I,J)+R(I+1,J))/DXW
       AIJ=-(AIM1J+AIJM1+AIJP1+AIP1J)
C....
       TB(IJ,IJ+1)=-AIJP1
       TB(IJ,IJ+JM)=-AIP1J
       TB(IJ,IJ-JM)=-AIM1J
       TB(IJ,IJ-1)=-AIJM1
       TB(IJ,IJ)=1.-AIJ
C      TB(IJ,IJ)=1.-(TB(IJ,IJ-JM)+TB(IJ,IJ-1)+TB(IJ,IJ+JM)+TB(IJ,IJ+1))
       IF(NT.EQ.1)THEN
       TA(IJ,1)=AIJP1
       TA(IJ,2)=AIP1J
       TA(IJ,3)=AIM1J
       TA(IJ,4)=AIJM1
       ENDIF
       TR(IJ)=TA(IJ,2)*TN1(IJ+JM)
     $        +TA(IJ,3)*TN1(IJ-JM)+TA(IJ,4)*TN1(IJ-1)
     $        +(1.-(TA(IJ,3)+TA(IJ,4)+TA(IJ,1)+TA(IJ,2)))*TN1(IJ)
C..SAVE FOR NEXT TIME STEP
       TA(IJ,1)=AIJP1
       TA(IJ,2)=AIP1J
       TA(IJ,3)=AIM1J
       TA(IJ,4)=AIJM1
C..
  110      CONTINUE
C..FOR I=1
       I=1
       DO 120 J=2,JM
       TJ=.5*(TN1(J)+TN1(J+JM))+TMPAIR
C........
       IJ=J
       IF(J.EQ.JM)THEN
       RM=RO3(I)
       ZM=ZO3(I)
       RP=RO3(I+1)
```

```
      ZP=ZO3(I+1)
      ELSE
      RM=.25*(R(I,J)+R(I,J+1)+R(I+1,J+1)+R(I+1,J))
      ZM=.25*(Z(I,J)+Z(I,J+1)+Z(I+1,J+1)+Z(I+1,J))
      RP=.25*(R(I+1,J)+R(I+1,J+1)+R(I+2,J+1)+R(I+2,J))
      ZP=.25*(Z(I+1,J)+Z(I+1,J+1)+Z(I+2,J+1)+Z(I+2,J))
      ENDIF
      DZ1=SQRT((RM-RP)**2+(ZM-ZP)**2)
      TB(IJ,IJ+JM)=1.-.5*COEFFH*DZ1/COEFKW
      TB(IJ,IJ)=-1.-.5*COEFFH*DZ1/COEFKW
      CONST1=.624*DZ1*COEFFH*ALAMDA*EWIS(J)*SX(J)/(COEFKW*CA)
      TR(IJ)=CONST1-TAIR*DZ1*COEFFH/COEFKW
  120      CONTINUE
C..FOR I=IM
      I=IM
      DO 130 J=2,JM
      IJ=(I-1)*JM+J
      IF(NT.GT.NTCI)THEN
      DO 135 JJ=2,JM
      IJ1=(I-1)*JM+JJ
      IJ2=(I-2)*JM+JJ
      IF(IJ1.NE.IJ)THEN
      TB(IJ,IJ1)=RKLS*W0(J-1,JJ-1)/DZ(JJ)
      TB(IJ,IJ2)=-RKLS*W0(J-1,JJ-1)/DZ(JJ)
      ELSE
      TB(IJ,IJ1)=.5+RKLS*W0(J-1,J-1)/DZ(JJ)
      TB(IJ,IJ2)=.5-RKLS*W0(J-1,J-1)/DZ(JJ)
      ENDIF
  135  CONTINUE
      DO 136 JJ=JM+1,JM+JE
      IJ3=(I-1)*JM+JJ
      TB(IJ,IJ3)=RHK*W0(J-1,JJ-1)
  136  CONTINUE
      TR(IJ)=RHS(J-1)
      SWJ=0.
      DO 137 JJ=2,JM+JE
      SWJ=SWJ+W0(J-1,JJ-1)
  137  CONTINUE
      TR(IJ)=TR(IJ)+(TSLD0-TMPAIR)*(1.+RHK*SWJ)
      ELSE
      TB(IJ,IJ)=1.
      TB(IJ,IJ-JM)=1.
      TR(IJ)=2.*(CT(J)-TMPAIR)
      ENDIF
  130      CONTINUE
C....FOR PTS ON SOLID EXPOSED SURFACE
      DO 150 J=JM+1,JM+JE
      IJ=(I-1)*JM+J
      IF(NT.GT.NTCS)THEN
      TB(IJ,IJ)=1.+RHK*W0(J-1,J-1)
      DO 155 JJ=2,JM
      IJ1=(I-1)*JM+JJ
      IJ2=(I-2)*JM+JJ
      TB(IJ,IJ1)=RKLS*W0(J-1,JJ-1)/DZ(JJ)
      TB(IJ,IJ2)=-RKLS*W0(J-1,JJ-1)/DZ(JJ)
  155    CONTINUE
      DO 156 JJ=JM+1,JM+JE
      IJ3=(I-1)*JM+JJ
      IF(IJ3.NE.IJ)TB(IJ,IJ3)=RHK*W0(J-1,JJ-1)
  156    CONTINUE
```

```
       TR(IJ)=RHS(J-1)
       SWJ=0.
       DO 157 JJ=2,JM+JE
       SWJ=SWJ+W0(J-1,JJ-1)
  157  CONTINUE
       TR(IJ)=TR(IJ)+(TSLD0-TMPAIR)*(1.+RHK*SWJ)
       ELSE
       TB(IJ,IJ)=1.
       TR(IJ)=TSLD0-TMPAIR
       ENDIF
  150     CONTINUE
C...FOR J=1. B.C. T(I,1)=T(I,2)
       J=1
       DO 140 I=1,IM
       IJ=(I-1)*JM+J
       TB(IJ,IJ)=1.
       TB(IJ,IJ+1)=-1.
       TR(IJ)=0.
  140       CONTINUE
C.....................................................
       CALL SOLVE(IM*JM+JE,TB,TR,TX,IWK,WK)
C...
       KT=0
       DO 300 IJ=1,IM*JM+JE
       TN1(IJ)=TX(IJ)
  300       CONTINUE
C...
       CALL SURF(DTIME,IM,JM,RR,VO,AA,R,Z,DVDT,
     $           EWIS,COEFFH,SX,RHOW,CA)
C.....................................................
       DO 417 KK=KNT,2,-1
       DO 417 II=1,JM+JE-1
       FTIM(II,KK)=FTIM(II,KK-1)
  417  CONTINUE
       DO 418 JJ=2,JM+JE
       J1=(IM-1)*JM+JJ
       J2=(IM-2)*JM+JJ
       I=IM
       FTIM(JJ-1,1)=-RHK*(TN1(J1)+TMPAIR-TSLD0)
  418  CONTINUE
C
       CALL NEXTR(NT,KNT,FTIM,RHS,TIME,W,F,WF,RS0)
C.....
       IF(DVDT*DTIME.GT.VO)GO TO 3
C.....................................................
   1       CONTINUE
C.....................................................
   2   STOP
       END
C...SUB. ASSIGNING THE CENTER PTS. FOR THOSE CELLS AT EDGE WHICH ARE
C...TRIANGLES.
       SUBROUTINE TRIO(IM,JM,R,Z,RO3,ZO3)
       DIMENSION R(IM+1,JM+1),Z(IM+1,JM+1)
       DIMENSION RO3(IM),ZO3(IM)
       J=JM
       DO 10 I=1,IM
       A=(.5*(Z(I,J)+Z(I,J+1))-Z(I+1,J))/
     $   (.5*(R(I,J)+R(I,J+1))-R(I+1,J))
       B=(.5*(Z(I+1,J)+Z(I,J+1))-Z(I,J))/
     $   (.5*(R(I+1,J)+R(I,J+1))-R(I,J))
```

```
      RO3(I)=(Z(I,J)-Z(I+1,J)+A*R(I+1,J)-B*R(I,J))/(A-B)
      ZO3(I)=Z(I,J)+B*(RO3(I)-R(I,J))
 10   CONTINUE
      RETURN
      END
C.....
      SUBROUTINE NEWSO(KK,IM,JM,R,Z,RO3,ZO3,I,J,RN,ZN,RE,ZE,
     $                 RW,ZW,RS,ZS,RO,ZO)
C
C....SUBROUTINE FOR ASSIGNING THE POSITIONS AT NORTH, EAST, WEST, SOUTH
C....CENTER OF  A CELL.
C....KK=4: CELL HAS FOUR SIDES; KK=3: CELL HAS THREE SIDES.
C....THE LEFT UPPER CORNER IS THE POSITION R(I,J) AND Z(I,J)
      DIMENSION R(IM+1,JM+1),Z(IM+1,JM+1)
      DIMENSION RO3(IM),ZO3(IM)
      IF(J.EQ.JM)THEN
      RO=RO3(I)
      ZO=ZO3(I)
      RN=RO3(I-1)
      ZN=ZO3(I-1)
      RS=RO3(I+1)
      ZS=ZO3(I+1)
      RW=.25*(R(I,J)+R(I,J-1)+R(I+1,J-1)+R(I+1,J))
      ZW=.25*(Z(I,J)+Z(I,J-1)+Z(I+1,J-1)+Z(I+1,J))
      ELSE
      RO=.25*(R(I,J)+R(I,J+1)+R(I+1,J+1)+R(I+1,J))
      ZO=.25*(Z(I,J)+Z(I,J+1)+Z(I+1,J+1)+Z(I+1,J))
      RE=.25*(R(I,J+1)+R(I,J+2)+R(I+1,J+2)+R(I+1,J+1))
      ZE=.25*(Z(I,J+1)+Z(I,J+2)+Z(I+1,J+2)+Z(I+1,J+1))
      RN=.25*(R(I,J+1)+R(I-1,J+1)+R(I-1,J)+R(I,J))
      ZN=.25*(Z(I,J+1)+Z(I-1,J+1)+Z(I-1,J)+Z(I,J))
      RW=.25*(R(I,J)+R(I,J-1)+R(I+1,J-1)+R(I+1,J))
      ZW=.25*(Z(I,J)+Z(I,J-1)+Z(I+1,J-1)+Z(I+1,J))
      RS=.25*(R(I+1,J)+R(I+1,J+1)+R(I+2,J+1)+R(I+2,J))
      ZS=.25*(Z(I+1,J)+Z(I+1,J+1)+Z(I+2,J+1)+Z(I+2,J))
      ENDIF
      RETURN
      END
C
      SUBROUTINE RZ90(IM,JM,RR,AA,R,Z)
C
C.....SUBROUTINE FOR ASSIGNING THE GRID POINTS.....
C.....R(I,J), Z(I,J): I=1,IM+1, J=1,JM+1
C.....IMAGINARY POINTS: 1) R(1,J), Z(1,J)
C                       2) R(IM+1,J), Z(IM+1,J)
C                       3) R(I,1), Z(I,1)
C.....AA: DROPLET HEIGHT; RR: DROPLET RADIUS.
      DIMENSION Z(IM+1,JM+1),R(IM+1,JM+1)
      RRR=AA/RR
C..
      DO 10 I=2,IM
      FI=1.-(I*1.-2.)/(IM*1.-2.)
      DO 10 J=2,JM
      GJ=(J*1.-2.)/(JM*1.-1.)
C..
      IF(I.EQ.IM.OR.J.EQ.2)THEN
      IF(I.EQ.IM)THEN
      R(I,J)=RR*GJ
      Z(I,J)=0.
      ENDIF
```

```
      IF(J.EQ.2)THEN
      R(I,J)=0.
      Z(I,J)=AA*FI
      ENDIF
C..
      ELSE
      FIR=1./(FI*RRR)-FI*RRR
      A=(1.+GJ**2+2.*(1.-GJ))*RR/FIR
      B=-2.*(GJ+(1.-GJ)/GJ)/FIR
      FACTOR=1.
      ELSE
      FACTOR=1.E-6
      ENDIF
      ALFA1=(1.+B**2)*FACTOR
      BEITA=2.*(A*B-(GJ+(1.-GJ)/GJ)*RR)*FACTOR
      GAMMA=(A**2+(GJ**2+2.*(1.-GJ))*RR**2)*FACTOR
      TF=BEITA**2-4.*ALFA1*GAMMA
      Z(I,J)=SQRT((1./(FI*RRR)+FI*RRR)**2/4.*RR**2-R(I,J)**2)
     $-(1./(FI*RRR)-FI*RRR)/2.*RR
 10       CONTINUE
      DO 20 I=1,IM+1
      R(I,JM+1)=RR
      Z(I,JM+1)=0.
 20       CONTINUE
C..FOR IMAGINARY POINTS
      DO 30 I=1,IM+1
      R(I,1)=-R(I,3)
     $+2.*R(I,2)
      Z(I,1)=Z(I,3)
 30       CONTINUE
      DO 40 J=1,JM
      R(IM+1,J)=R(IM-1,J)
      Z(IM+1,J)=-Z(IM-1,J)
     $+2.*Z(IM,J)
 40       CONTINUE
      I=1
      AA1=AA+(Z(2,2)-Z(3,2))
      RRR=AA1/RR
      FI=1.
      Z(I,2)=FI*AA1
      DO 50 J=3,JM
      GJ=(J*1.-2.)/(JM*1.-1.)
      FIR=1./(FI*RRR)-FI*RRR
      A=(1.+GJ**2+2.*(1.-GJ))*RR/FIR
      B=-2.*(GJ+(1.-GJ)/GJ)/FIR
      IF(FIR.GT.1.E-3)THEN
      FACTOR=1.
      ELSE
      FACTOR=1.E-6
      ENDIF
      ALFA1=(1.+B**2)*FACTOR
      BEITA=2.*(A*B-(GJ+(1.-GJ)/GJ)*RR)*FACTOR
      GAMMA=(A**2+(GJ**2+2.*(1.-GJ))*RR**2)*FACTOR
      TF=BEITA**2-4.*ALFA1*GAMMA
      IF(TF.LT.0.)TF=0.
      Z(I,J)=SQRT((1./(FI*RRR)+FI*RRR)**2/4.*RR**2-R(I,J)**2)
     $-(1./(FI*RRR)-FI*RRR)/2.*RR
 50       CONTINUE
      R(1,1)=-R(1,3)+2.*R(1,2)
      Z(1,1)=Z(1,3)
```

```
C....
       RETURN
       END
C
       SUBROUTINE DZ0(IM,JM,R,Z,RO3,ZO3,DZ)
C
C....SUBROUTINE FOR FINDING THE DZ
       DIMENSION R(IM+1,JM+1),Z(IM+1,JM+1),DZ(JM)
       DIMENSION RO3(IM),ZO3(IM)
       I=IM
       DO 135 JJ=2,JM
       IF(JJ.EQ.JM)THEN
       RM=RO3(I)
       ZM=ZO3(I)
       RP=RO3(I-1)
       ZP=ZO3(I-1)
       ELSE
       RM=.25*(R(I,JJ)+R(I,JJ+1)+R(I+1,JJ+1)+R(I+1,JJ))
       ZM=.25*(Z(I,JJ)+Z(I,JJ+1)+Z(I+1,JJ+1)+Z(I+1,JJ))
       RP=.25*(R(I-1,JJ)+R(I-1,JJ+1)+R(I,JJ+1)+R(I,JJ))
       ZP=.25*(Z(I-1,JJ)+Z(I-1,JJ+1)+Z(I,JJ+1)+Z(I,JJ))
       ENDIF
       DZ(JJ)=SQRT((RM-RP)**2+(ZM-ZP)**2)
  135    CONTINUE
       RETURN
       END
C
       SUBROUTINE SOLVE(N,A,B,X,IWK,WK)
C
C.....SUBROUTINE FOR SOLVING MATRIX
C...'LINK XXX,SOLVE,IMSL/LIB'....
       DIMENSION A(N,N),B(N),X(N)
       DIMENSION IWK(N),WK(N+N*(N-1)/2)
       INTEGER N
       CALL L2NRG(N,A,N,A,N,WK,IWK)
       DO 100 J=1,N
       X(J)=0.0
       DO 100 I=1,N
       X(J)=X(J)+A(J,I)*B(I)
 100   CONTINUE
       RETURN
       END
C
       SUBROUTINE SURF(DTIME,IM,JM,RR,VO,AA,R,Z,DVDT,
     $                 EWIS,COEFFH,SX,RHOW,CA)
C
C.....SUBROUTINE FOR CALCULATING THE SIZE OF THE LIQUID DROP RR, AA
C.....WHILE RR IS A CONSTANT
C
        DIMENSION R(1+IM,1+JM),Z(1+IM,1+JM),EWIS(JM),SX(JM)
        COMMON /MATER/ LMAT
C...REMEMBER TN1+TEMP0 IS THE REAL TEMP. FOR EVALUATING THE PROPERTIES.
       PI=4.*ATAN(1.)
       SSX=0.
       DO 10 J=2,JM
       RJ=.5*(R(2,J)+R(2,J+1))
       DRJ=SQRT((R(2,J+1)-R(2,J))**2+(Z(2,J+1)-Z(2,J))**2)
       SSX=SSX+EWIS(J)*COEFFH*SX(J)*RJ*DRJ
  10     CONTINUE
       DVDT=2.*PI*.624/(RHOW*CA)*SSX
```

```
      VO=VO-DVDT*DTIME
      BETA=RR/EXP(1./3.*LOG(.75*VO/PI))
      P1=1./2.
      P2=1./3.
      U=EXP(1./3.*LOG(3.*VO/PI+SQRT(RR**6+9./PI**2*VO**2)))
      AA=U-RR**2/U
      RETURN
      END
C
        SUBROUTINE NEXTR(NT,KT,FTIM,R,TIME,W,F,WF,RS0)
C
        DIMENSION W(NP,NP),F(NP),FTIM(NP,KT)
        DIMENSION WF(NP),R(NP),RS0(NP+1)
        COMMON /CONST/ ALFA,PI
        COMMON /GRID/ DR0,DT0,NDP,NP,TN
        COMMON /INTG/ AT0,ERRREL,IRULE
        COMMON /MATER/ LMAT
        DO 149 II=1,NP
        R(II)=0.
149      CONTINUE
        IF(NT.LE.KT)THEN
        KKT=NT
        ELSE
        KKT=KT
        ENDIF
        DO 150 IT=1,KKT
C   SELECT PROPER WEIGHTS
        T0=IT*DT0
C..
        CALL WEIGHT(T0,W,RS0)
C   PICK UP CORRESPONDING FLUX
        DO 100 I=1,NP
        F(I)=FTIM(I,IT)
100     CONTINUE
C
C   SUMMATION IN SPACE
        CALL MULT(NP,NP,W,F,WF)
C   SUMMATION IN TIME
        CALL ADD(NP,WF,R)
150     CONTINUE
        RETURN
        END
C
        SUBROUTINE MULT(M,N,W,F,WF)
C
        REAL W(M,N),F(N),WF(N)
C
        DO 50 I=1,M
        WF(I)=0.0
        DO 50 K=1,N
        WF(I)=WF(I)+W(I,K)*F(K)
50      CONTINUE
        RETURN
        END
C
        SUBROUTINE ADD(NP,WF,R)
C
        REAL WF(NP),R(NP)
C
        DO 50 I=1,NP
```

```
            R(I)=R(I)+WF(I)
   50       CONTINUE
            RETURN
            END
C
            SUBROUTINE WEIGHT(T0,W,RS0)
C
            REAL W(NP,NP),RS0(NP+1)
            REAL QDAG,BSI0E,ERF
            EXTERNAL F1
C
            COMMON /CONST/ ALFA,PI
            COMMON /GRID/ DR0,DT0,NDP,NP,TN
07800
            COMMON /INTG/ AT0,ERRREL,IRULE
            COMMON /RR0/ R,R0
            COMMON /MATER/ LMAT
C
            DO 50 I=1,NP
            DO 50 J=1,NP
            DR0=RS0(J+1)-RS0(J)
            R=.5*(RS0(I+1)+RS0(I))
            R0=.5*(RS0(J+1)+RS0(J))
*    SET UP (W) FOR T0 < DT0
            ERRABS=0.0
            IF(T0.LT.DT0)THEN
            W(I,J)=QDAG(F1,AT0,0.5,ERRABS,ERRREL,IRULE,RESULT,ERREST)
            W(I,J)=RESULT
            END IF
*
*    SET UP (W) FOR T0 > DT0
            IF(T0.GE.DT0)THEN
            ARG1=DR0/SQRT(16*ALFA*T0)
            ARG3=(R-R0)**2/(4*ALFA*T0)
            ARG4=0.5*R*R0/(ALFA*T0)
            IF(I.NE.J)THEN
            W(I,J)=(1.0/SQRT(4.0*PI*ALFA))*R0*(T0**(-1.5))*
     &           BSI0E(ARG4)*EXP(-ARG3)*DR0*DT0
            ELSE
            W(I,J)=(R/T0)*BSI0E(ARG4)*ERF(ARG1)*DT0
            END IF
            END IF
*
   50       CONTINUE
            RETURN
            END
C
            FUNCTION F1(T0)
            REAL BSI0E,ERF
            COMMON /CONST/ ALFA,PI
            COMMON /GRID/ DR0,DT0,NP
            COMMON /RR0/ R,R0
C
            ARG1=DR0/SQRT(16*ALFA*T0)
            ARG3=(R-R0)**2/(4*ALFA*T0)
            ARG4=0.5*R*R0/(ALFA*T0)
            E=0.0
            IF(ARG3.LE.80.0)E=EXP(-ARG3)
            IF(R.NE.R0)THEN
            F1=(1.0/SQRT(4.0*PI*ALFA))*R0*(T0**(-1.5))*
```

```
     &      BSI0E(ARG4)*E*DR0
            ELSE
            F1=(R/T0)*BSI0E(ARG4)*ERF(ARG1)
            END IF
            RETURN
            END
C
           SUBROUTINE CTEMP0(IM,JM,JE,TREF,TWATER,TSOLID,CT)
C
C...SUBROUTINE CALCULATING THE CONTACT TEMPERATURE TO BE USED AT
C...THE SOLID-LIQUID INTERFACE
           DIMENSION TWATER(IM*JM+JE),CT(JM)
           COMMON /SOLID/ SK,SC,SR
           COMMON /WATER/ COEFKW,CPW,RHOW
C......
           SQRCKW=SQRT(RHOW*CPW*COEFKW)
           SQRCKA=SQRT(SR*SC*SK)
C....
           DO 10 J=1,JM
           CT(J)=(SQRCKW*(TWATER((IM-2)*JM+J)+TREF)
     $                    +SQRCKA*TSOLID)/(SQRCKW+SQRCKA)
  10       CONTINUE
           RETURN
           END
C.....SUB. FOR ASSIGNING POINTS ON SOLID SURFACE
           SUBROUTINE RSD(JM,JS,RR,RS0)
           DIMENSION RS0(JM+4*JS)
           DR1=RR/(1.*JM-1.)
           DO 10 J=1,JM
           RS0(J)=(J-1.)*DR1
  10       CONTINUE
           RS0(JM+1)=RS0(JM)+DR1
           DO 20 J=JM+2,JM+JS
           RS0(J)=RS0(J-1)+DR1
  20       CONTINUE
           DO 30 J=JM+JS+1,JM+2*JS
           RS0(J)=RS0(J-1)+2.*DR1
  30       CONTINUE
           DO 40 J=JM+2*JS+1,JM+3*JS
           RS0(J)=RS0(J-1)+4.*DR1
  40       CONTINUE
           DO 50 J=JM+3*JS+1,JM+4*JS
           RS0(J)=RS0(J-1)+8.*DR1
  50       CONTINUE
           RETURN
           END
```

8. REFERENCES

M. di Marzo, A. K. Trehan, "Transient Cooling of a Hot Surface by Droplet Evaporation",National Bureau of Standards Report, NBS-GCR-86-516, 1986

M. di Marzo, D. D. Evans, "Evaporation of a Water Droplet Deposited on a Hot High Conductivity Solid Surface", National Bureau of Standards Interagency/Internal Report, NBSIR 86-3384, 1986

M. di Marzo, Z. Y. Wang, W. H. Meng, "Transient Cooling of a Hot Surface by Droplets Evaporation", National Bureau of Standards Report, NBS-GCR-87-534, 1987

M. di Marzo, D. D. Evans, A. K. Trehan, "The Cooling Effect of a Single Droplet on a Hot Semi-Infinite Metal Body", National Bureau of Standards Interagency/Internal Report, NBSIR 87-3517, 1987

M. di Marzo, D. D. Evans, "Dropwise Evaporative Cooling of High Thermal Conductivity Materials", Heat and Technology, Vol. 5, No. 1-2, pp. 126-136, 1987.

M. di Marzo, D. D. Evans, "Evaporation of a Water Droplet Deposited on a Hot High Thermal Conductivity Solid Surface", The Transaction of the American Society of Mechanical Engineers, Journal of Heat Transfer, in press

W. H. McAdams, Heat Transmission, 3rd ed., McGraw-Hill, New York, 1957

M. Seki, H. Kawamura, K. Sanokawa, "Transient Temperature Profile of a Hot Wall Due to an Impinging Liquid Droplet", Journal of Heat Transfer, Vol.100, 167, 1978.

NIST-114
(REV. 9-92)
ADMAN 4.09

U.S. DEPARTMENT OF COMMERCE
NATIONAL INSTITUTE OF STANDARDS AND TECHNOLOGY

MANUSCRIPT REVIEW AND APPROVAL

(ERB USE ONLY)
ERB CONTROL NUMBER | DIVISION
PUBLICATION REPORT NUMBER: NIST-GCR-93-622 | CATEGORY CODE

INSTRUCTIONS: ATTACH ORIGINAL OF THIS FORM TO ONE (1) COPY OF MANUSCRIPT AND SEND TO: THE SECRETARY, APPROPRIATE EDITORIAL REVIEW BOARD.

PUBLICATION DATE: April 1993 | NUMBER PRINTED PAGES

TITLE AND SUBTITLE (CITE IN FULL)

TRANSIENT COOLING OF A HOT SURFACE BY DROPLETS EVAPORATION

CONTRACT OR GRANT NUMBER
70NANB8H0840

TYPE OF REPORT AND/OR PERIOD COVERED
Final Report, November 1990

AUTHOR(S) (LAST NAME, FIRST INITIAL, SECOND INITIAL)
P. Tartarini, Y. Liao, M. di Marzo
University of Maryland
Mechanical Engineering Department
College Park, MD 20742

PERFORMING ORGANIZATION (CHECK (X) ONE BOX)
[ ] NIST/GAITHERSBURG
[ ] NIST/BOULDER
[ ] JILA/BOULDER

LABORATORY AND DIVISION NAMES (FIRST NIST AUTHOR ONLY)

SPONSORING ORGANIZATION NAME AND COMPLETE ADDRESS (STREET, CITY, STATE, ZIP)
U.S. Department of Commerce
National Institute of Standard and Technology
Gaithersburg, MD 20899

RECOMMENDED FOR NIST PUBLICATION

[ ]	JOURNAL OF RESEARCH (NIST JRES)	[ ]	MONOGRAPH (NIST MN)	[ ]	LETTER CIRCULAR
[ ]	J. PHYS. & CHEM. REF. DATA (JPCRD)	[ ]	NATL. STD. REF. DATA SERIES (NIST NSRDS)	[ ]	BUILDING SCIENCE SERIES
[ ]	HANDBOOK (NIST HB)	[ ]	FEDERAL INF. PROCESS. STDS. (NIST FIPS)	[ ]	PRODUCT STANDARDS
[ ]	SPECIAL PUBLICATION (NIST SP)	[ ]	LIST OF PUBLICATIONS (NIST LP)	[X]	OTHER NIST-GCR
[ ]	TECHNICAL NOTE (NIST TN)	[ ]	NIST INTERAGENCY/INTERNAL REPORT (NISTIR)		

RECOMMENDED FOR NON-NIST PUBLICATION (CITE FULLY) [ ] U.S. [ ] FOREIGN

PUBLISHING MEDIUM
[X] PAPER [ ] CD-ROM
[ ] DISKETTE (SPECIFY)
[ ] OTHER (SPECIFY)

SUPPLEMENTARY NOTES

ABSTRACT (A 1500-CHARACTER OR LESS FACTUAL SUMMARY OF MOST SIGNIFICANT INFORMATION. IF DOCUMENT INCLUDES A SIGNIFICANT BIBLIOGRAPHY OR LITERATURE SURVEY, CITE IT HERE. SPELL OUT ACRONYMS ON FIRST REFERENCE.) (CONTINUE ON SEPARATE PAGE, IF NECESSARY.)

This report describes the research performed during the period July 1989 - July 1990 under a joint research program between the Mechanical Engineering Department of the University of Maryland and the Center for Fire Research of the National Institute of Standards and Technology. The research is conducted by Graduate Research Assistants of the ME Department under the joint supervision of Dr. di Marzo (UMCP) and of Dr. Evans (CFR - NIST). A new experimental set-up for the study of dropwise evaporation in a radiant heat transfer field has been designed, constructed and tested. The various issues of concern such as: steady state solid temperature distribution, radiant heater design and configuration, infrared background noise and post test data manipulation are outlined.

KEY WORDS (MAXIMUM 9 KEY WORDS; 28 CHARACTERS AND SPACES EACH; ALPHABETICAL ORDER; CAPITALIZE ONLY PROPER NAMES)

aluminum; computer programs; cooling; droplets; evaporation; solid surfaces; water

AVAILABILITY
[X] UNLIMITED [ ] FOR OFFICIAL DISTRIBUTION. DO NOT RELEASE TO NTIS.
[ ] ORDER FROM SUPERINTENDENT OF DOCUMENTS, U.S. GPO, WASHINGTON, D.C. 20402
[X] ORDER FROM NTIS, SPRINGFIELD, VA 22161

NOTE TO AUTHOR(S) IF YOU DO NOT WISH THIS MANUSCRIPT ANNOUNCED BEFORE PUBLICATION, PLEASE CHECK HERE. [ ]

LECTRONIC FORM